NUCLEAR REACTIONS WITH A PROTON MAGNETIC SPECTROGRAPH

Thesis by

Cheng Wu Li

In Partial Fulfillment of the Requirements

For the Degree of

Doctor of Philosophy

California Institute of Technology

Pasadena, California

1951

ACKNOWLEDGMENTS

To Professors Charles C. Lauritsen and W. A. Fowler I wish to express my deep appreciation for the privilege of working with them, for their active assistance and helpful discussions and for their continued friendly interest in my progress. I also wish to thank Professors R. F. Christy and T. Lauritsen for valuable advice and consultations.

Dr. Ward Whaling, as my coworker, has played a leading part in many of the experiments. To him, I am especially indebted for numerous suggestions and discussions, from the planning of an experiment to the linguistic side of this thesis.

To the many colleagues in the Kellogg Laboratory and many senior graduate students, it is with much appreciation that I wish to acknowledge their assistance and discussions during my work in this laboratory.

ABSTRACT

A double-focussing, semicircular sector, magnetic spectrograph has been constructed for detecting and analyzing charged particles from nuclear reactions, with energy up to 10 Mev for protons and alpha particles. Particles emitted at a point outside the field and within a solid angle of 0.007 steradian can be brought to a point focus, also outside the magnet, by the magnetic field which varies as $r^{-\frac{1}{2}}$ near an average radius of 16 inches. The ultimate momentum resolution $p/\delta p$ limited by the second order aberrations and other irregularities of the actual arrangement is over 1000. With the $\frac{1}{4}$ inch collecting slit usually employed for intensity measurement, the momentum resolution is $p/\delta p = 230$.

The magnetic spectrograph has been used to determine accurately the energy release in a number of nuclear reactions initiated by protons or deuterons on Li^7, Be^9, B^{11}, C^{13}, N^{15} and O^{16}. These measurements, incorporated with the great number of accurate disintegration energy measurements recently available, have been used to derive the masses of light nuclei up to F^{20} from the nuclear data exclusively.

TABLE OF CONTENTS

LIST OF TABLES

LIST OF FIGURES

PART I

INTRODUCTION

With the recent improvement in the production of accurately monoenergetic ion beams, the precise analysis of the energy and accurate measurement of the yield of nuclear reaction products becomes increasingly important in order to elucidate the structure and behaviour of atomic nuclei. To achieve these objects an analyzer with high dispersion and energy resolution and with large solid angle is required. Among the reaction products, heavy charged-particles form a special group. They can be accurately analyzed by methods of electric or magnetic deflection. For magnetic deflection, the non-ferromagnetic type spectrometers so useful for electrons are usually not practical for heavy charged-particles because of the enormous magnetizing current necessary to deflect appreciably a heavy particle of a few Mev. Among the ferromagnetic type there are the uniform field, single-focussing spectrometers and the inhomogeneous field, double-focussing spectrometers. The first class is astigmatic, gives a line image of a point source and has very limited aperture. The second class is anastigmatic, forms a point image and has increased aperture with dispersion twice that of the first class.

On the other hand, the first class gives an extended spectrum at a given magnetic field, suitable for photographic registration; and the uniform magnetic field can be measured absolutely, without trouble in calibration. Buechner has built such a 180 degree uniform field magnet and succeeded in measuring Q values very well; although he does

not think it is suitable for yield measurements. The second class gives a point image of particles with a definite energy at a given magnetic field. The energy spectrum of the particles is obtained by changing the focussing magnetic field continually. If yield measurements are wanted in addition to energy measurements or if detection by counters are to be used, the second class seems to be indicated.

Thus it is evident that the choice to a double-focussing proton (or other heavy charged-particles) magnetic spectrograph was dictated by the possibility of obtaining a magnetic field that is strong enough to focus the usual, energetic heavy charged-particles from nuclear reactions and the possibility of obtaining large aperture for yield measurements. For electrons, several double-focussing spectrometers have been constructed and the priniciple has been extensively discussed in the literature. The first double-focussing proton spectrograph was completed in this laboratory recently, capable of focussing protons up to 2 Mev[1]. The instrument is a modification of the design of Siegbahn and Svartholm[2] for electrons, employing a ring-shaped inhomogeneous magnetic field having the property of double-focussing. The ring extends to 180° instead of the full coverage of $(2\pi)^{\frac{1}{2}}$ radians or 254.56°, to enable both the source and collector to be located outside the field. The present model, designed by Sylvan Rubin, is the second of this type of magnetic spectrograph; many features of the first model, as well as many empirical considerations from experience, have been incorporated. The main difference is in the use of the internal flux path of the magnetizing coils for focussing the particles instead of exposing the focussing to the outside with the coils wound around a core. With its present dimensions, this spectrograph is capable of focussing protons up to 10 Mev.

The important functions of such a spectrograph has been summarized by Snyder et al.[1]. With the resent design, determination of a number of nuclear reaction Q values has been made, yielding results with an error as small as 1 part in 1,500 or 0.07% of energy. The Q values agree excellently with those by Buechner's group, who used a uniform field spectrometer and photographic registration; the accuracy is comparable (Table II or IV). The most important Q values are $Li^7(p,\alpha)He^4$, $C^{13}(d,\alpha)B^{11}$ and $O^{16}(d,\alpha)N^{14}$ which are the key reactions in the determination of nuclear masses. Hithertofore, the mass spectrographs serve to determine the main mass scale; no substantial portion of the mass table could be derived from nuclear disintegration data alone. With the Q values of $C^{13}(d,\alpha)B^{11}$ and $O^{16}(d,\alpha)N^{14}$ well established, it is now possible to derive the masses of light nuclei from nuclear data completely. A first trial of this derivation has been made (Part IV) and yielded significant results.

In addition, cross-sections of several reactions have been calculated from the measurements. The agreement of the cross section of $Li^7(p,\alpha)He^4$ with the results of previous investigators was one of the first indications of the reliability of the instrument. Some weak groups of particles have been observed. Another experiment which has been done with the spectrograph is on the alpha spectrum of $Li^8(\beta^-)2He^4$ and $B^{11}(p,\alpha)2He^4$, the analysis of which will furnish additional information on the 2.8 Mev excited state of Be^8. These results will be reported elsewhere.

Many experiments can be conceived immediately utilize the spectrograph with its high resolution and large aperture. And it seems that the full capabliity of this kind of instrument is not yet recognized.

Many investigations are yet to be done. In this connection, mobility of the instrument will be one of the practical problems to be solved.

PART II

THE MAGNETIC SPECTROGRAPH

THEORETICAL CONSIDERATIONS

Several double-focussing spectrometers for electrons, and recently one for heavy particles, have been built and the principle has been extensively discussed in the literature[1-10]. The works by Judd[8] on theoretical considerations and by Snyder, Rubin, Fowler and Lauritsen[1] on the first proton magnetic spectrograph are especially pertinent to the present discussion. For convenience of reference, a summary of results of the theoretical investigations is given in the following, with the constants of the recent design as illustration.

The Focussing Field.

A magnetic field is required which has cylindrical symmetry about the z-axis and mirror symmetry about the plane z = 0, the "midplane", in cylindrical coordinates. For an anastigmatic image, the radial component of the field must vanish in the midplane and the axial component must vary as $r^{-\frac{1}{2}}$ in the vicinity of a particular circle $r = r_0$ which we shall designate as the "midcircle". When the magnetic field is extensive enough, the conjugate foci lie on the midcircle, separated by an angular distance of $(2\pi)^{\frac{1}{2}}$ radian or 254.56° [2]. In the present design, the pole pieces are only 180 degrees in extent, and a first order focus is still obtained in this case, although some dispersion and resolution, for a given solid angle, is sacrificed. To a first approximation the foci are found by linear extrapolation beyond the pole pieces of the trajectories

inside the field. The spectrograph can then be considered as a thick spherical lens and the usual optical theory applied.

Constants of the Magnetic Spectrograph.

The constants of the present design as a magnetic lens, calculated from theory, are illustrated in Fig.1.

The radius of midcircle: $r_o = 16$ inches.

The angular extent of the magnetic field: $\theta = 180^o$.

Focal length, the distance between focal planes and unit planes:

$$f = f' = \sqrt{2}r_o \csc \theta/\sqrt{2} = 1.78r_o = 28.5 \text{ inches.}$$

Distances of unit planes from ends of pole pieces, measured inward:

$$u = u' = \sqrt{2}r_o \tan \theta/\sqrt{2} = 2.86r_o = 45.8 \text{ inches.}$$

Distances of focal planes from ends of pole pieces, measured inward:

$$g = g' = -\sqrt{2}r_o \cot \theta/\sqrt{2} = 1.08r_o = 17.3 \text{ inches.}$$

The conjugate focal points, object and image, can be determined from either of the standard relations:

$$\frac{1}{e} + \frac{1}{e'} = \frac{1}{f} \quad ; \quad ff' = xx' \tag{1}$$

where e and e' are measured from the unit planes and x and x' from the focal planes. Also, it has been shown that the image distance, d', measured outward from the end of the pole pieces, directly in terms of the object distance, d, similarly measured, is

$$d' = -\sqrt{2}r_o \tan(\theta/\sqrt{2} + \tan^{-1} d/\sqrt{2}r_o)$$

$$= -22.6 \tan(127.28^o + \tan^{-1} d/22.6) \text{ inches.} \tag{2}$$

Using an object distance d = 17.5 in., we have d'=6.1". Visually we got a good focus at 5.5 in. from the end of the pole pieces with no apparent astigmatism. At d = 29.3", d' = 0, and at d = 0, d' = 29.3".

The first order anastigmatic image also shows no distortion and the magnification in both the r and z direction is

$$\begin{aligned} M &= \left(d/\sqrt{2}r_o \sin\theta/\sqrt{2} - \cos\theta/\sqrt{2} \right)^{-1} \\ &= d'/\sqrt{2}r_o \sin\theta/\sqrt{2} - \cos\theta/\sqrt{2} \\ &= \left(0.562\, d/r_o + 0.606 \right)^{-1} \\ &= 0.562\, d'/r_o + 0.606. \end{aligned} \tag{3}$$

For $d = 17.5"$, $r_o = 16"$, this gives $M = 0.82$.

The dispersion of the instrument is

$$D = \frac{\frac{\delta r}{r_o}}{\frac{\delta P}{P_o}} = \frac{\frac{\delta r}{r_o}}{\frac{\delta H}{H_o}} = \frac{1+M}{1-n} = 2(1+M) \tag{4}$$

where δr is a small increment in the image position measured normal to the optic axis of the spectrograph arising from a change δP in the momentum of the particles injected into the spectrograph or from a change H in the magnetic field H of the spectrograph. We note that $D = 2(1+M)$ for the anastigmatic spectrograph as compared with $D = 1+M$ for the type with uniform field ($n = 0$). In the present arrangement of the spectrograph, $D = 3.6$.

The ultimate resolving power of the instrument is limited by higher order calculations, fringing field effects and the actual construction of the instrument. For source and collector sizes large compared to the ultimate image size, the resolution can be computed from the width of the collecting slit, δr_c, by using the expression for D given above. For the case described here,

$$R_c = \frac{P_o}{\delta P_c} = \frac{D r_o}{\delta r_c} = 3.6\left(\frac{r_o}{\delta r_c}\right). \tag{5}$$

For a finite source width, δr_s, a similar expression is obtained by

replacing δr_c by δr_s, yielding

$$R_s = \frac{P_o}{\delta P_s} = \frac{1+M^{-1}}{1-n}(r_o/\delta r_s) = 4.4(r_o/\delta r_s). \qquad (6)$$

The solid angle over which the emitting particles from a point source can be collected by the instrument depends on the object distance and is given by

$$\Omega = \frac{A}{2r_o^2 + d^2} \text{ steradians.} \qquad (7)$$

In the present arrangement, the cross sectional area of the vacuum chamber, $A \simeq 8$ sq. in., $r_o = 16$ in., $d = 17.5$ in., we have $\Omega = 0.01$ steradian. Experimentally, we found it to be 0.007 steradian.

DESIGN, CONSTRUCTION AND PERFORMANCE

Essential Parameters.

The dimensions of the present spectrograph, as designed by Sylvan Rubin, was so chosen as would be able to focus protons and alpha particles of energy up to 10 Mev, such as produced by most nuclear reactions with incident particles of a few Mev. Pole pieces 180 degrees in extent were used for easy access to the source and collector. Also, 180 degrees is convenient from the standpoint of construction, since it allows simultaneous machining of the contours of both pole faces, and also other parts of the magnet. The choice of a 180° sector represents a reasonable compromise between the conflicting requirements as discussed by previous investigators.

The magnetizing coils were wound around the pole pieces instead of around the core as in the first model of double-focussing

magnetic spectrograph built in this laboratory. The magnetic circuit is completely in iron except for the gap, so that one is using the internal path of the magnetic flux at the vital place and increases the usable proton energy with a given dimensions. Such windings also diminish the effect ofexternal magnetic sources, as well as the leakage flux, and make the spectrograph magnetically isolated or insulated from the surroundings.

The radius is 16 inches so that a field of 11,000 gauss would be required to focus protons or alpha particles of 10 Mev. With the use of internal magnetic path it was believed that such a field could be attained in a gap of 2 inches in the magnetic circuit by 50,000 ampere turns of magnetizing current.

The Magnet Body.

The steel body which forms the magnetic flux path consists of (Figure 2):

(The words height and width refer to the position when the magnet body was lying flat on the floor, not established on the framework as in use now).

(1) two pole pieces -- height 3.50", O.D. 19", width 6" each; rounded at the corners;

(2) two pole faces -- height at the central circle: 0.750", O.D. 19", width 6" each (see the section Shaping of the Magnetic Field), rounded at the corners;

(3) two inner returns -- combined height 10.50", O.D. 20.5";

(4) one outer return, which forms the "back" of the magnet -- height 10.50", O.D. 47.5", width (thickness) 2";

(5) two "inner" yokes -- O.D. 47.5", height 3" each;

(6) two "outer" yokes -- O.D. 32", height 2" each.

Remember that the radius of midcircle is 16", the gap between the pole faces at the midcircle is 2", and all pieces are 180° sectors. Pole faces were made of Armco iron, the other parts were all made of hot rolled steel, annealed. Matched pieces were machined simultaneously by fastening them to a steel base to form a complete circle. The pieces were threaded at proper places for assembly. The total weight of these parts is about 2300 lbs. The complete assembly has the appearance of a steel block of the shape of a short semicircular cylinder, weighing about two and a half tons. The outer yokes were added so that the magnetic flux will more evenly distribute itself through the outer and inner returns and eliminate the constriction of the magnetic path at the intersections of the pole pieces with the inner yokes.

Figure 3 gives the front view of the magnet and Figure 4, the back view. The magnet is supported with four adjustable single-ball bearings and screws attached to a steel shaft made of angle bars and I-bars. Mobility is provided by a system of six pads on which the 5000 lbs. magnet rests. These pads sit on a sanded smooth steel plate, 3/16 " x 10' x 6'. Oil can be blown into these pads with the laboratory compressed air line (about 70 psi) until air begins to escape with oil between the O-rings at the bottom of the pads and the steel plate, so that the magnet is essentially supported on a film of oil and can be moved about over the steel plate. Some trouble in distributing the weight evenly over the six pads has been experienced and perhaps a more satisfactory method of moving the magnet could be devised. The magnet has been moved around within a room and recently to another room satisfactorily.

Shaping of the Magnetic Field.

To achieve the desired field variation of $r^{-\frac{1}{2}}$ required for anastigmatism, a first approximation calculation indicated that the pole

faces should have a slope

$$\left|\frac{\partial z}{\partial r}\right| = \left|\frac{nz_o}{r_o}\right| = \frac{1}{2}\left|\frac{z_o}{r_o}\right|$$

where (r_o, z_o, θ) is the midcircle right on the surface of a pole face. In our case, $r_o = 16"$, $z_o = 1"$, hence

$$\left|\frac{\partial z}{\partial r}\right| = \frac{1}{32} .$$

And the pole faces should make an angle of $1^o47'$ with the plane z = constant. Lips must be provided along the inner (r = min.) and the outer (r = max.) edges of the pole faces to compensate the leakage of magnetic flux. In the first model, these lips occupy about half of the total width ($r_{max} - r_{min}$) of 3 inches. In the present design, each inner lip makes an angle 9^o to the plane z = constant, extending from r = 13" to 13.6"; and each outer lip makes an angle of 14^o to the plane z = constant, extending from r = 18.5" to 19". Thus the cross section of a pole face has the following shape:

r:	13"	13.6"	16"	18.5"	19"
height:	0.921"	0.825"	0.750"	0.672"	0.797"

After the assembly of the magnet body and the coils, measurements were made by H. H. Woodbury at an average field of 1200 gauss with flip coils put inside the hole on the back and a Grassot fluxmeter. The absolute values of this kind of measurement are certainly not very accurate, but relative measurements are much better. The field in the gap is very close to the desired $r^{-\frac{1}{2}}$ variation from r = 13.8" to 18.2". Closer inspection shows that: (1) regarded as a straight line on the log-log graph, the exponent n in the expression r^{-n} is a little less than $\frac{1}{2}$; and (2) besides the general falling-down of field near both edges (outside the range r = 13.8" to 18.2"), there seems to be some deviation from a

straight line within the range r = 13.8" to 18.2", to lower fields at the high field side and to higher fields at the low field side. As a matter of fact, the whole profile of the field distribution must be a continuous curve with continuously changing slope. Hence we can as well include (2) in (1) and say that the usable portion is a straight line with n a little smaller than $\frac{1}{2}$.

From theoretical considerations, the astigmatism introduced by n being smaller than $\frac{1}{2}$ is that the focal length for trajectories in the midplane with r varying is shorter than the focal length for trajectories in the cylinder $r = r_o$ with z varying. With the collector system now in use, the slit is parallel to the axis of the cylindrical coordinates and thus is parallel to the z-focal line. Accordingly, to get a sharper image, or more exactly, to get the maximum momentum resolution, the slit should be located at the r-focal point, coincident with the z-focal line, and long enough to accommodate the whole z-focal line. Such a position is nearer to the end of the pole piece than the image point given by d' in Eq. (2) for the case $n = \frac{1}{2}$ exactly.

The above discussion shows that a small deviation of n from $\frac{1}{2}$ is not serious so far as momentum resolution is concerned if a suitable collecting arrangement can be made. First order theory of Judd shows that the resolution increases and the solid angle decreases as n increases, and the solid angle is much less sensitive than resolution to small changes in the exponent n, which indicates that there may be an advantage in choosing n somewhat greater than $\frac{1}{2}$ for applications requiring large resolution, if a line collector, not a strict point collector, can be used. Thus if correction were to be made on our magnet, an over correction might be advantageous.

As to the effect of this deviation of n from $\frac{1}{2}$ on the other aberrations, as well as the second order aberrations of the $n = \frac{1}{2}$ case, no investigation has been made. Presumably they are of the same order of magnitude. So are the effects of the fringing field, the changing of the permeability of iron with the field, the position of magnetizing coils and other discrepancies between ideal and practically attainable fields. Actually, all these effects will be interrelated and defy rigorous mathematical analysis.

It is believed that better fit to $n = \frac{1}{2}$ than we have can be attained after a few trial cuts, but also that the present dimensions are pretty good, probably within 0.010" of the best values. As to the actual performance of the present instrument, no apparent astigmatism has been seen on a scintillation screen by visual observation and the focussing behaviour has been quite satisfactory to our purpose and the ultimate resolution has seldom been used. Thus, no further studies on field distribution and focussing properties nor mechanical modifications in the pole faces contours have been made. Of course, whether a mere change in n to make it closer to $\frac{1}{2}$ will improve the focussing properties is still a question.

Magnetizing Coils.

One unconventional point in the present design is the winding of the magnetizing coils around the pole pieces instead of around a core. Sixteen kidney shaped coils were connected in series to form the magnetizing circuit. Flat copper wire of cross section 0.094" x 0.375", coated with heavy formvar, was used. Each coil was wound manually with a jig around a wooden dummy of the pole piece fastened on a turn table. Copper wire was wound around and pushed against the dummy with several supports

and hammered to keep the flat side of the wire in close contact with each preceding turn. The winding started from somewhere on the back of the C shaped dummy and proceeded inside out. Each coil has approximately 25 turns. One coil was wound clockwise, the next one counterclockwise, and the two were soldered together at the starting points. In this manner coils were connected to form 6 double-layer coils. The remaining 4 were single-layer coils. Each double-layer or single-layer coil was wrapped with half-inch wide cotton ribbon, varnished and dried. In assembly, these coils were interposed with cooling coils of similar shape and slided around each pole piece, in the following manner: single -- cooling -- double -- cooling -- double -- cooling -- double -- cooling -- single -- inner yoke. A sheet of empire cloth was placed between each cooling coil and the adjacent coil, the interspace liberally spread with insulating varnish; a sheet of thick fish paper between the inner yoke and the sidemost layer of coil. After baking, insulation from coils to ground and between coils has been checked from time to time and is well over 20 megohms.

The sixteen coils have about 400 turns altogether and a total length of about 4000 feet. The total resistance at room temperature is 1.0 ohm. An increase in temperature of 50°C will raise the resistance by 20%. A reading in the voltmeter and ammeter for the magnet current furnishes a convenient indication of the resistance of the wire, and therefore the approximate temperature of the coils. Because there may be hot spots in certain part of the conductor, the temperature may be assumed to be 50% higher than that indicated by the meter readings, as a safe measure.

Fig. 6 shows the magnetic field produced in the gap as a function of the magnetizing current. This current is supplied by a

d-c generator of 35 kw. and 120 volts output. Grid-iron type resistors of 1 and 2 ohms are used to reduce the magnet current but keep the generator running at stable voltages, when a low magnetic field is wanted.

Cooling.

The magnet is water-cooled by coils of copper tubing, having the same shape as the magnetizing coils. Copper tubing of 3/8 " O.D. was first moderately flattened by passing through a rolling machine. Two pieces of flattened tubing put side by side with the flattened part lying on the turntable were wound around the wooden model used before. Then the two pieces were connected at two of the ends by soldering with a short length of curved tubing, leaving the other two ends free for entrance and exit of water. Tin solder was spread liberally over several places of the finished coil, then ground with a flexible grinding plate to make it even. In assembly, eight such coils were connected in parallel to two manifolds which were connected to the laboratory water line through high pressure rubber hoses.

The cooling has been found to be not very efficient. During a run, with three gallons per minute of water flow, when the temperature of the magnetizing coils may be as high as 40°C above the room temperature as indicated by the change in resistance, the water flowing out is only about 10°C above the room temperature. The temperature rise in the magnetizing coils is about 60°C after 5 minutes at 130 amperes, with a 20°C rise in the temperature of the exit cooling water. This inefficiency in heat exchange is evidently due to too much insulation. Not only is there the intervention of much insulating material but also that most part of the cooling coil is far from the insulated magnetizing coils, even though the cooling tubing has been flattened somewhat.

The highest field available with the generator now in use is able to focus protons of about 9 Mev. With a larger power supply, a field capable of focussing 10 Mev protons can certainly be maintained for continuous operation, without heating the coils too much. The coils can stand a temperature of 150°C safely; they were raised to this temperature during the baking after the assembly. With better cooling, the upper limit of focussable proton energy could very likely be pushed still higher, since the saturation effects apparently do not impair the focussing properties.

If better contact between the conductors and the cooling elements could be made, the heat exchange would have been much better. Cooling plates provided with grooves for circulating tubings like that used in the first model may be more effective than this design. Or the space between the conductor and cooling elements can be filled with insulating material of better thermal conductivity. Internal water-cooling or other direct-contact cooling of the conductor is also possible. Intermittent operation of the magnet has been practiced in some of the experiments.

To estimate the temperature of the coils, besides the indication given by the ammeter and voltmeter across the magnet coils, a thermocouple indicator has been attached to the side of the coils. A better arrangement will be to attach a thermocouple indicator in direct contact with each coil to indicate the temperature of each coil. The location of these indicators may be worth consideration too. Incidently, removable blocks on the back or other part of the magnet would be very convenient in attaching accessories, placing the fluxmeter, detecting and mending leaks of the vacuum chamber, etc.

Vacuum Chamber and Pumping System.

The vacuum chamber was made of two half brass shells, silver-soldered with a well-fitted brass guiding strip locked into grooves machined on the edges of the two half shells. It is fitted tightly in the gap between the pole faces and has the same general shape as the gap. The inside cross-section of the chamber, about 4.9" x 1.7", is of barrel shape. Two necks made of 2" brass pipe project outward from the ends of pole pieces for making connection to the target chamber and the detector. A hole at the back of the chamber provides the pumping path. A small well of 1-1/8 " diameter and 2-5/8 " deep at one corner of the chamber, equivalent to r = 14", was originally designed for housing the fluxmeter coil and is not in use now because of very nonlinear saturation effects at this place. Moreover, it was found to cast a little shadow into the usable path of the protons with the source at 17.5" from the end of the pole pieces. The finished vacuum chamber can slide in and out the gap just by loosening the assembling screws a little.

The volume of the chamber is about 500 cubic inches, without any narrow constriction. A two stage diffusion pump with a forepump, and conventional pirani and ionization gauges complete the vacuum system. The diffusion pump is attached to the back of the vacuum chamber and is water-cooled with a pressurestat control. The pump might be put near one of the ends of the vacuum chamber instead of the middle of the back, leaving the latter for arranging fluxmeter, etc.

The Fluxmeter.

As originally designed, the small well mentioned above, which extends into one end of the vacuum chamber, provided a space for the fluxmeter coil. This has turned out to be more of a problem than

we had anticipated. In this position, at r = 14", the fluxmeter coil was in a field which is stronger than at the midcircle r_o = 16", or the stable, non-oscillating orbit, but it was expected that the field measured by the fluxmeter would be proportional to the field at the stable orbit, i.e., proportional to the momentum of particles. It was found that the field measured by the fluxmeter did not increase proportionately with the particle momentum, and at 10,500 gauss it was 1.5% too low in comparison with 8,500 gauss. This changing of the magnetic field distribution does not impair the resolution, as indicated by the width of the 8.78 Mev alpha line of ThC'; however, it is very inconvenient so far as energy measurements are concerned, since it requires that the fluxmeter be calibrated with particles of accurately known energy.

Several modifications of the fluxmeter used in the first model[1] have been built to fit in the well, with good sensitivity. After the problem of nonlinearity appeared, many suggestions and several trials have been made about the method and the place of measuring the field. At last we have placed the fluxmeter in the middle of the back of the magnet, fitting it in the pipe connecting the diffusion pump to the vacuum chamber with the fluxmeter coil centered accurately at r = 16", the supposed stable orbit. Since this coil projects right into the middle of the path of the particles, some of them must be intercepted. We estimate that the effective aperture is reduced by less than 5%. Because of many physical limitations, it is the simplest way we have found capable of measuring the non-uniform field with sufficient accuracy. Some nonlinearity of the field measurements still exists and needs calibration, which will be discussed below. With this calibration, the measurements given by the fluxmeter are quite satisfactory.

The fluxmeter coil consists of a single layer of 40 turns of No. 32 magnet wire on a thin aluminum form, 7/8 " in diameter, cemented with DeKhotinsky cement to a few inches of 1/16 " brass wire and then to a long 3/32 " brass tubing, which was the lightest material readily available. The tubing is supported by two glass V bearings, embedded near the axis of the tubing, each upon a tungsten pivot ground from 0.020" tungsten wire and cemented eccentrically in the end of a screw mounted on a horizon al brass beam of $\frac{1}{4}$" x $\frac{1}{4}$" so that the distance between the tungsten pivots can be adjusted by turning the screws. The beam is soldered perpendicular to the cover of the 3" T which connects the diffusion pump to the pipe leading into the vacuum chamber. The cover of the T is directly opposite the hole on the back of the vacuum chamber, so that one can try to look into the dark interior of the vacuum chamber through the peep holes on the cover. A small mirror on the movable brass tubing and a prism-mirror system bring the reflected image of the filament of a lamp on to a ground glass screen. The image of the filament serves as the indicator. A cross bar of stiff quartz-fiber, two and a half inches long, with a weight of one third of a gram attached to one end, put through the brass tubing horizontally, supplies a constant balancing torque. Stops have been fixed above and below the free end of the cross bar. The leads from the fluxmeter coil are connected to fine pigtails, 1.5" lengths of 1.5 mil copper strip. The current used in the fluxmeter coil to produce the electromagnetic torque is usually from 10 to 50 milliamperes, supplied by dry batteries, and measured by a precision potentiometer on the potential drop across a resistor of 1, 2, or 5 ohms, in series with the fluxmeter coil.

One trouble with this arrangement is that the vapour of pump oil gradually condenses on the mirror and makes the reflected image

very dim and the vacuum must be opened and the mirror cleaned from time to time. The oil vapour even causes the quartz cross fiber to stick to the stops. No collection of electrostatic charge on the coil form, which is insulated from the tubing, has been observed. Heating of the coil sometimes makes the current drift but causes no serious trouble. Damping is good and the period of oscillation of the movable part short, so that the indicator can be brought to the mark satisfactorily during adjustment of the field.

In this arrangement, the current required in the fluxmeter coil to produce the electromagnetic torque in an average field H, to balance the constant torque of the weight, is

$$I \propto \frac{1}{H}$$

where I is the magnitude of the current as given in terms of millivolts of potential drop across the resistor in series with the fluxmeter coil.

During a run, keeping I constant, the field H is regulated, by manually adjusting the field current in the generator supplying the magnet, to keep the indicator of the fluxmeter within the mark, just two parallel lines on the ground glass screen. The magnetic field can be varied by steps as small as 1 in 2000. With close watch, the field can be kept constant to 1 part in 5,000; 1 part in 2,000 is easy to maintain. No measurements have been made to determine how quick the generator current, the magnetic field and the fluxmeter indicator on the screen respond to the adjustment and to each other. But the sensitivity of the fluxmeter is better indicated by the points on Fig. 9, the ThC' alpha line which has been used for calibration. Fig. 7 shows two groups of alpha particles from ThC, the peaks corresponding to energy 6.0425 Mev and 6.0817 Mev.

The ThC' source, prepared by the capture of recoils from the decay of thoron on a highly polished aluminum electrode, 1/16 " in diameter, was mounted on the target holder so that it could be moved quickly into the target position without disturbing the apparatus. Care was taken to see that in the preparation of the targets none of the evaporating material was deposited on this source; the ThC' spectrum was observed both before and after each evaporation and if the two energy readings did not agree the source was discarded. New sources were prepared frequently. The energy of the alpha particles from ThC' is given by Briggs(12) as 8.7759 ± 0.0009 Mev. The energy of the alphas from our source will be less than this because the ThC' atoms are imbedded in the source backing as a result of the recoil of the ThB nuclei into the source. After the method given by Rutherford(13) we calculate the range of the ThB recoil to be 0.136 mm air equivalent, and estimate the average alpha energy loss in the source to be 4.4 kev, with a probable error of 25%. The peak in the ThC' spectrum thus represents an energy of 8.7715 ± 0.002 Mev. Another standard of the field measurement is the Po alpha particles of 5.2987 ± 0.001 Mev.

During each period of experiment, calibrations are made frequently, usually several times within four or five hours. The probable average wandering of the fluxmeter calibration from the peak of the natural alpha line in a period of experiment (four or five hours), regarded as an experimental quantity, has been found from many such periods of experiment, to about 1 in 7,000. This quantity was taken to be the statistical probable error of any point taken from a curve consisting of a number of fluxmeter readings.

During the run, the calibration appeared to shift a little when the magnet was warming up. Therefore, before starting an experiment, current was allowed to run for half an hour or so to heat the magnet to its steady temperature. No attempt has been made to determine the shift in calibration in a long period, because it is unnecessary and because the vacuum has often been opened and the fluxmeter taken out from time to time.

To mention a few other possible ways of measuring the field which have been considered and may still be worth considering: First, the fluxmeter well at the end of the vacuum chamber can still be used if suitable energy calibration, for example, from electrostatic generator of sufficient energy range, can be made. Or, the well may be omitted, or moved to the other side of the stable orbit, at r = 18" instead of r = 14", where the well would be in a lower field with saturation effects less acute and it would no longer obstruct the usable aperture as in our present arrangement. At both these positions, the field distribution is far from symmetrical, and hence not only a torque but also a linear force would be exerted on a coil put in these positions. Another recommendation made by Professor C. C. Lauritsen is to cut the vacuum chamber down from 180° to about 150°, extending the pipe at the end into the region between the pole pieces. With this arrangement, a large fluxmeter coil could be placed around the pipe, avoiding any interference with the trajectories of particles. A simple proton magnetic moment resonance arrangement has been tried, put into the back hole of the magnet. We also tried to shim the non-homogeneous magnetic field with iron material to make it more uniform locally. It is believed, with the proton resonance circuits now available, the non-homogeneity of the field is no longer a serious problem, but the location of the proton moment fluxmeter would still present

serious difficulties.

The Momentum Scale of the Fluxmeter, Nonlinearity of Field Measurements.

From the inverse relation between I and H or the momentum of the particles being focussed, it can be shown that the particle energy is

$$E \approx \frac{C_m Z^2}{\left(M_o + \frac{E}{2c^2}\right) I^2} \approx \frac{C_m Z^2}{M_o I^2}\left(1 - \frac{E}{2M_o c^2}\right),$$

where M_o is the mass of the particle focussed by the spectrograph and the term $E/2c^2$ is a small relativistic correction. For a fluxmeter whose reading is exactly linear in the momentum scale, the spectrograph constant C_m would be a constant. However, it was found, in the present arrangement of the fluxmeter, that C_m is not exactly a constant, though not far from it. Fig. 8 shows a plot of C_m against the energy of particles. This is obtained essentially from four points: (1) ThC' alphas at 8.8 Mev(12,14), (2) ThC alphas at 6 Mev, (3) Po alphas at 5.3 Mev, and (4) the average point of elastically scattered protons and deuterons of energy around 1 Mev from various targets at a known angle. Although the energy of the incident particles for the point (4) has been very accurately determined, the average point itself is rather smeared out because of the different experiments with varying accuracies which are involved in this point.

The deviation of C_m from a constant in the energy range 1 to 9 Mev is about 1%. It is interesting that C_m changes slowly but continuously as the field is changing. C_m decreases as H increases. With the fluxmeter in its old position, within the well at about r = 14" near the end of the pole pieces, it measured a field at 10,500 gauss (for energy 8.8 Mev) that was 3% too low in comparison with a field of 8,500 gauss (for energy 6 Mev). In that case, C_m would be 3% higher for 8.8 Mev than that for 6 Mev; and that means, C_m increases as H increases. In the

present position of the fluxmeter, in the middle of the gap, it seems to measure a field rigidity $H\rho$ that is higher than it should be to be proportional to the particle momentum.

Why the magnet behaves in such a manner is not very clear to us. A tentative explanation may be this: Refer to Fig. 5, the field distribution in the gap along the radial direction. At low field, assume the portion of usable field is represented by a straight line on the graph. Due to the change in permeability of iron with the field, the left side of the straight line, which is the high field side, does not increase so fast with the magnetizing current as the right side or the low field side. Hence the straight line becomes more horizontal and at the same time curves down at its left side gradually as the magnetizing current increases. Thus n becomes increasingly smaller than $\frac{1}{2}$ and the usable portion of the straight line becomes narrower and shifts to the right, i.e., to larger r. Now consider the same coordinate system as before, in which $r = 0$ is the geometrical center of the magnet. Because of the decrease in n, a trajectory of the particle is more convex than the corresponding trajectory in an $n = \frac{1}{2}$ field, and the middle of the average path of the particles from the source to the collector shifts to a point $r = r_2 > 16"$ at field H_2, while the center of curvature shifts to a point $r = r_1 > 0$, with the result that the product $H_2(r_2 - r_1)$ becomes increasingly smaller than the product $H_o r_o$, where H_o is the field at $r = r_o = 16"$. Although the difference $H_2 r_2 - H_o r_o = (1 - n)H_o \delta r = (1 - n)H_o(r_2 - r_o)$ is positive for any $n < 1$, but the momentum of the focussed particles is essentially determined by the field rigidity H of the average path which is $H_2(r_2 - r_1)$ at the middle of the path, and the apparent momentum given by the fluxmeter reading corresponds to the quantity $H_o r_o$. Therefore, the fluxmeter measures too high a $H\rho$ compared to the average momentum of the collected

particles.

If the above explanation is correct, it would be an additional reason for overcorrecting the pole faces to make n a little larger than $\frac{1}{2}$ at low average field; however, other explanations are not excluded. For example, the fluxmeter may change its configuration or its position relative to the magnet as the temperature of the magnet or the flux coil changes. Or the real cause may be composed of many factors. Evidently it is hard to judge without actual trials the best point to put the fluxmeter to measure the average field, and it seems very probable we can by no means get awayfrom some nonlinearity of momentum scale of the fluxmeter in a ferromagnetically produced non-homogeneous field, because a constant field distribution required by a linear momentum scale needs a constant permeability of iron across the whole width of the pole faces. The use of materials of better magnetic properties, for example, the use of Armco iron throughout the magnet body, may somewhat improve the situation but it does not seem to be possible to remove these saturation effects completely.

Fringing Field, Saturation Effects and Focussing Behaviour.

The present spectrograph is magnetically a self-contained unit. The measurements made by this instrument are not affected by large stray fields in the laboratory. Also it produces very little stray field itself. The operation of source and detector in the vicinity of the spectrograph is very convenient. Photo-multiplier tube with some iron shielding has often been used for the detector. The only places where the field fringes out are at the entrance and exit of the magnetic gap. This fringing field deflects the protons through the the apparatus by $3\frac{1}{2}$ degrees at each end, so that the total deflection is 187°, instead of 180°. When the field in the gap is 5000 gauss,

measurements of the field near the entrance end give the following result, where the distance was measured from the end of the pole pieces outward, along the line tangent to the midcircle:

distance	-2"	-1"	0	1"	2"	3"	4"	5"
field	100%	98%	80%	40%	18%	9%	4%	2%

The percentage is relative to 5000 gauss. The field produced by the magnetizing coils themselves is in a direction opposite to the fringing field of the magnet, and at a distance of 12" from the magnet on the tangent line to the midcircle, the fringing field is only 3 gauss, or about 0.1% of the field in the gap.

The principal effect of the fringing field is to displace the focal points. However, since the fringing does not vary as $r^{-\frac{1}{2}}$, it also introduces astigmatism. On the first model built in this laboratory, the fringing field is very large. It bends particles through about 6^{o} after they leave the magnet and the observed astigmatism is attributed to this field. It has been empirically found that the astigmatism can be made negligibly small by making the distance from source to magnet much larger than the distance from the detector to magnet, and the very large fringing field of the first model does not impair its focussing behaviour seriously. In the present design, the fringing field has been greatly reduced. Although accurate measurements have been made with only one source and image position, it can be sure that other arrangements, not necessary with image distance considerably smaller than the object distance as in the first model, will be satisfactory. For instance, a symmetrical arrangement can be used, which will increase the available solid angle.

Saturation phenomena have been described above in connection with the fluxmeter positions and the nonlinearity of its momentum scale.

Better than expected, the gradual saturation and change in field distribution does not seem to impair the focussing properties noticeably.

The image was first found from visual observation in darkness of Po alphas focussed on a ZnS screen. The source of 1 millicurie activity was 1/16 " in diameter. There was no apparent astigmatism at the image distance d' = 5.5". At that position, the image on the screen was about 2 mm. in diameter to the naked eye, a pear-shaped spot with the pointed end directed along r increasing, with some background scintillations scattered all over the screen. With the screen fixed and the source position changing, the image changed to an irregular, more or less rectangular patch of dim light, about 3/4 " high and $\frac{1}{2}$" across.

Resolution.

The theoretical resolution of the present set up has been mentioned above. For a $\frac{1}{4}$" collecting slit, the momentum resolution has been calculated to be $p/\delta p = 230$, and for a 1/32 " collecting slit, $p/\delta p = 1840$.

The actual ultimate resolution is best indicated by the observed width of some of the natural alpha lines (Fig. 7 & 9). Using a 1/32 " collecting slit, for the 8.778 Mev alpha line from ThC' source of 1/16 " size, we find a width at half maximum smaller than 20 kev, equivalent to a momentum spread of $p = p/900$. Po and ThC alpha lines give the same kind of spread. The theoretical image size of the source would be 1/20 ", equivalent to a momentum spread of p/1150. Thus the width of the line is roughly equal to that due to the image size, and we can conclude that the ultimate limit of resolution of the instrument

is better than $p/\delta p = 1000$. Even if we assume the source to be a point, we find that the extra width of the line, in addition to the slit width of p/1840, is only

$$\sqrt{\left(\frac{p}{900}\right)^2 - \left(\frac{p}{1840}\right)^2} \approx \frac{p}{1000}$$

This extra width of p/1000 may also include the source thickness. The experimental resolution can also be estimated from the observed slope $I/\delta I$ of the front edge of a thick target curve for scattering of mono-energetic particles(1) with similar conclusion about the resolution. A good demonstration of the resolution has been given by the scattering curve of protons from surface layer of O and C on thin Be foil.

During experiments 1/32 " collecting slit has been chiefly used for calibration; the $\frac{1}{4}$" collecting slit is generally used for measuring the energy distribution of the emitted particles.

Scattering Angular Extent and Solid Angle.

With the target position now in use, and without any aperture stop, the mean horizontal angular spread of the accepted particles has been measured to be about 4° by Rutherford scattering of protons from copper with a slit which subtended an angle of 0.4° at the source and could be rotated around the source. It is evident from these measurements that the fluxmeter well eclipses a little into the way of the particles. Moreover, the cross section of the vacuum chamber is barrel shaped. The plot of the Rutherford scattering against the angular position of the slit is shaped roughly like the letter "M", with a dent at the top representing the shadow of the fluxmeter well. An angular extent of $2\frac{1}{2}$ degrees on the top can be estimated as the flat part.

The vertical angular aperture has not been measured. A

comparison of measured value of this angle with the value computed from the geometry of the vacuum chamber will be interesting too.

The solid angle of the present design, from the Rutherford scattering cross section and by direct comparison of the number of Po alpha particles collected by the spectrograph from a source of known strength, has been found to be 0.007 steradian, in contrast to the theoretical value of 0.01 steradian.

A summary of the theoretical and experimental characteristics of the spectrograph follows:

Table I. Summary of the characteristics of the spectrograph.

		Theoretical	Experimental
r_o	main radius	16"	
θ	angular extent of field	180°	187°
n	field variation in r^{-n}	$\frac{1}{2}$	slightly less than $\frac{1}{2}$
f = f'	focal length	28.5"	
g = g'	distance of focal planes inside ends of pole pieces	17.3"	
d	object distance	17.5"	
d'	image distance	6.1"	5.5"
M	magnification	0.8	
D	dispersion	3.6	
R	momentum resolution: with $\frac{1}{4}$" slit	230	
	with 1/32 " slit	1840	> 900
	ultimate		>1000
$\Delta\theta$	scattering angular extent (horizontal)		4°
Ω	solid angle	0.01	0.007

EXPERIMENTAL SET UP

Source of Incident Particles.

The Institute 1.5 Mev pressure-insulated electrostatic accelerator with the precision electrostatic analyzer[15,16] has been used to supply proton and deuteron beams. Both H^+ and HHH^+ have been used. The energy of the particles can be fixed monoenergetic to better than 0.2 kev at 1.0 Mev when careful alignment of the beam is maintained. During the course of work the calibration of the analyzer was checked frequently against the $F^{19}(p,\gamma)$ resonance at 873.5 ± 1 kev and the $Al^{27}(p,\gamma)$ resonance at 993.3 ± 1 kev[17]. Usually an accuracy of 0.1% was assigned as the statistical probable error of the energy of the incident particles and another 0.1% as systematic error due to the uncertainty in the standards. With a first-order relativistic correction, the energy E of the incident particles in terms of R, the reading of the potential across the electrostatic analyzer, is given by

$$E\left(1+\frac{E}{2M_0c^2}\right) = C_e Z R \ ,$$

or

$$E = C_e\left(1-\frac{E}{2M_0c^2}\right) Z R \ ,$$

where M_0 is the rest mass and Z the charge of the particle, and C_e is the analyzer constant.

Target Chamber.

The target chamber consists of: a 3" height x 4" diameter cylindrical scattering space, three steel tubes connected toward the source side and one toward the magnet, a furnace and a liquid-air cold trap. It was attached to the magnetic spectrograph through a flexible sylphon bellows. The sylphon was rigidly fixed by auxiliary screws and

steel supports after the position of the target chamber relative to the magnet had been adjusted to give the best visual image of a Po source at the target position on a scintillation screen fixed at 5.5" from the other end of the magnet. Three entrance ports to be connected to the source side have been provided at scattering angle of 60°, 90°, and 120° roughly. Only the angle 90° has been used and measured, more exactly, to be 89.3° ± 0.2°. The connection to the source side was made by a small sylphon to the tubing which forms the exit path of the particles coming out of the electrostatic analyzer. A convenient beam interrupter made of a meniscus-shaped piece of iron sheet was hung freely inside the lucite portion of the connecting tubing and operated by a small a.c. transformer with an iron core to form an electromagnet. The beam interrupter is so shaped and placed as will cut off the beam when it is attracted by the electromagnet and otherwise will swing out of the way by its own weight. Several adjustable slits were made of short length of small brass tubing with a hole in each. They serve to align the beam and control the width of the beam striking the target. A quartz disc can be moved into the path for visual observation.

The target position now in use, 17.5" from the end of magnet, was chosen to provide the maximum space around the target, in particular, so that the incident beam can be brought in at a wide range of angles. The 4" cylinder which housed the target was made of steel. A 1" x 2" quarz plate with fine mark on it was fitted on the side of the cylinder directly opposite the beam entrance, useful especially in the alignment of the beam so that the scattering angle is fixed. The target holder is located eccentrically to the cylinder, near the quartz window, to facilitate gamma ray measurements. A calibration source can be mounted in a 1/16" hole on the target holder and put into the target position by lowering the target holder. At the bottom of the cylinder is the

liquid-air cold trap, a stainless steel can of 2" diameter and 6" depth. Two copper rods extend from the top cover of the cylinder to the bottom part of the can. A strip of 0.003" or 0.005" tantalum sheet across the ends of the copper rods form the furnace. Sometimes tungsten wires were used as the furnace. The furnace is water-cooled by spirals of small copper tubings soldered around the exposed ends of the copper rods which also serve as the leads of heating current. The latter ranged from tens of amperes to 150 amperes. The target can be lowered into the bottom of the cold trap, near the furnace to receive the evaporated material. In the tubing on the magnet side of the scattering chamber is a piece of brass with an accurately-machined rectangular hole, $1\frac{1}{2}$" x 1", which acts as the entrance aperture to the magnet. The opening of this aperture can be adjusted by turning the knob outside, to which a protractor is attached.

Collection and Detection.

A set of horizontal slits of width, 1/32 ", 1/16 ", 1/8 " and $\frac{1}{4}$" respectively, in a brass plate, can be moved into the image position. Quick change in slit width is necessary since calibration requires a very narrow slit with high resolution and detection of reaction products generally requires a wide slit with increased intensity.

The particles were detected either by a proportional counter or a scintillation counter. The latter uses ZnS phosphor and RCA 5819 electron multiplier within iron shielding. A linear pulse amplifier with adjustable rise time[18] has been used in conjunction with a variable bias Schmitt discriminator and the usual decade scalers and a register, controlled by an automatic relay system driven from the beam current integrator.

Measurement of Angle.

The angle θ between the direction of the incident beam and the direction in which emitted particles leaving the target enter the spectrograph must be known accurately to determine the Q value from the observed particle energies. This angle was measured by two independent methods: (1) by the ratio of the energies of monoenergetic protons elastically scattered from Be and Ta targets, which gives a value of θ independent of the bombarding energy; and (2) by means of a stop with a narrow slit in it which could be rotated about the target to intercept first the incident protons and then the particles entering the spectrograph. The angle through which the slit turned was read from a dividing head fixed to it. Both methods agree within 0.1 degree and show the angle of observation to be 89.3 degrees; a probable error of 0.2 degree has been assigned.

Before the above measurements a direct optical measurement gave the angle 89.5 degrees, but later on the set up of the slits in the target chamber had been changed a little and this method of measurement has not been used again.

PART III

THE DETERMINATION OF ENERGY RELEASE IN NUCLEAR REACTIONS

The double-focussing magnetic spectrograph described above has been used to analyze the reaction products and determine the energy release in a number of nuclear reactions initiated by monoenergetic proton and deuteron beams from the 1.5 Mev electrostatic generator. The targets include Li^7, Be^9, B^{11}, C^{13}, N^{15} and O^{16} and the measured particles include protons, deuterons, tritons and alpha particles with energy ranging from 1 Mev of scattered particles to about 9 Mev for alpha particles from $Li^7(p,\alpha)He^4$.

The standard expression giving the reaction energy Q in terms of the various parameters involved is:

$$Q = \left(1 + \frac{M_2}{M_3}\right) E_2 - \left(1 - \frac{M_1}{M_3}\right) E_1 - \frac{2(M_1 M_2)^{\frac{1}{2}}}{M_3} (E_1 E_2)^{\frac{1}{2}} \cos\theta$$

where the M's are nuclear masses with relativistic corrections. The determination of E_1, E_2 and θ has been described above. Energy measurements have also been discussed by Snyder, Rubin, Fowler and Lauritsen[1]. The method of calculation of Q from the observed data with necessary corrections and the estimation of errors has been dealt with by Brown et al.[10]. The following reactions are studied:

(1) $Li^7(p,\alpha)He^4$

(2) $Be^9(d,\alpha)Li^7$

(3) $B^{11}(p,\alpha)Be^8$

(4) $C^{13}(d,\alpha)B^{11}$

(5) $C^{13}(d,\alpha)B^{11*}$

(6) $C^{13}(d,t)C^{12}$

(7) $C^{13}(d,p)C^{14}$

(8) $N^{15}(p,\alpha)C^{12}$

(9) $O^{16}(d,\alpha)N^{14}$

A brief discussion on the reactions is given below, followed by tables giving a summary of the Q values and the analysis of systematic and statistical errors.

(1) $Li^7(p,\alpha)He^4$ and (2) $Be^9(d,\alpha)Li^7$

Both thick and thin targets of lithium metal, evaporated in vacuum on copper backings, were used. Fig. 9 shows typical thin and thick target spectra, together with the alpha spectrum from ThC' source located in the target position. The energy scale is fixed by the peak in the ThC' curve. For the thick target curve the energy of the alphas coming from the surface of the target was taken to be that of a point at 54% the maximum thick target yield, indicated by the arrow in the figure. This 54% value was chosen by considering the shape of the curve obtained by folding the spectrograph window into the spectrum for infinite resolution, and is higher than the customary midpoint as a result of the rapid variation of the reaction cross-section with proton energy, and the relatively low resolution employed with the thick targets, $p/\delta p = 230$. For the thin target the peak in the curve was corrected, in the usual way, by adding to the peak energy one-half the thickness of the target measured in units of alpha particle energy. The target thickness was found from the integrated thin target yield by comparison with the yield from an infinitely thick target.

Three determinations of Q were made at a bombarding energy of 1008 kev using H^+ ions and eight at 336 kev using HHH^+ ions. At the

lower bombarding energy the Li alpha particle energy is very close to that of the ThC' alpha particles, and by calibrating the fluxmeter with the ThC' alphas, errors that might arise from inaccuracies in the field measurement are avoided. At the higher bombarding energy a slight correction for the non-linearity of the field measurement by the fluxmeter was added. At the higher bombarding energy the effect of surface contamination layers is smaller, but the effect of the uncertainty in the angle of observation is relatively more important. The values of Q at these two energies checked to within 3 kev and have been averaged to give the value of 17.338 ± 0.011 Mev. The 11 kev uncertainty is the probable error in Q arising from the experimental errors listed in Table III. The statistical error in the average value of Q was calculated in two ways: (1) from the deviations in individual Q measurements from the average of Q; (2) from a compounding of the items in a detailed analysis of the statistical errors listed in Table III; and it turned out that (1) and (2) agree to less than 1 kev. The systematic errors were taken as listed in Table III.

Care was taken to see that in the preparation of the Li targets none of the metal was deposited on the source of ThC' used for calibration of the field measurements; the ThC' alpha spectrum was observed both before and after each evaporation and if the two energy readings did not agree the source was discarded. New sources were prepared frequently, five different sources were used in the eleven determinations of Q.

The observed energy of the alpha particles has been corrected for the energy loss of incident and emitted particles in the surface layers of carbon and oxygen that appeared on the target surface during bombardment. The way in which these layers built upon a clean Li surface

as a function of the bombarding charge was first determined, measuring the thickness of the layers by observing the protons elastically scattered from them. Then the surface layer on each target used was estimated from its total bombarding charge. Some uncertainty arises from the fact that the various points on the curve were taken after different amounts of bombarding charge. However, since on the average the thickness of both carbon and oxygen layers together amounted to only about 1 kev for 336 kev protons, measured normal to the surface, the effect of this uncertainty on the final value of Q is very small.

This value of Q is higher than the previously accepted value of 17.280 ± 0.030 Mev, determined from range measurements(20). This discrepancy may be accounted for in part by the surface layers or possibly to an error in the measurement of the angle of observation, which seems difficult to know accurately in the earlier experiment. This new value is in excellent agreement with a similar magnetic measurement by Buechner (Table IV) whose value is 17.340 ± 0.014 Mev.

The reaction $Be^9(d,\alpha)Li^7$ has been measured with the same procedure described above. Beryllium foils were used as targets. The magnetic spectrograph was calibrated against Po alpha particles. The average of six determinations with both thick and thin beryllium targets is 7.151 ± 0.010 Mev, in agreement with Buechner's value of 7.150 ± 0.008 Mev, though not with the recent value of Klema, 7.191 ± 0.024 Mev (Table IV). This Q value can also be calculated from the experimental Q values of $Be^9(p,\alpha)Li^6$ and $Li^6(d,p)Li^7$ which give 7.152 ± 0.010 Mev (Table IV).

(3) $B^{11}(p,\alpha)Be^8$

Targets were prepared by evaporating boric acid (H_3BO_3) in the furnace. This compound loses its crystal water at low temperature with

continuous heating and becomes boric oxide (B_2O_3) which is known to boil at 1230°C. At 60 amperes of heating current, several minutes were needed to drive off the crystal water. After this, 60 amperes of current for several seconds at a bright whitish-yellow heat was sufficient to give a good target on clean copper backing. The thickness of the target was first estimated by the shift of the step curve of the protons elastically scattered from the copper backing after the evaporation as compared with before. If the target was used, the thickness of the target, when it is thin, was calculated more accurately by comparison with the thick target yield. The tantalum furnace frequently cracked while cooling after evaporation. A flat piece of tantalum was found to last longer than other shapes. Four runs were made with a new target each time. Three were thin targets and one thick. Another thick target was prepared by pressing amorphous boron on copper backing. We also succeeded in evaporating amorphous boron with a heating current of 160 amperes, but no measurement has been made with it.

The small peak of alpha particles from the ground state is just at the tail of the large peak of the alpha particles leaving Be^8 at 2.8 Mev excited state. The ratio of total intensities of these two groups were found to be 1 to 35. But with the bombarding energy of 1.006 Mev, apparently not many counts in the small peak were due to the tail of the large peak (Fig. 10).

The following table gives the individual Q measurements. Better values than these could be obtained by more careful procedure. The average value 8.574 ± 0.014 is in good agreement with that of Buechner's group, 8.567 ± 0.011 Mev (Table IV).

Target material	Target thickness to outgoing alphas	E_1 (Mev)	E_2 (Mev)
B_2O_3	75 kev	1.006	6.322
B_2O_3	98 kev	1.006	6.333
B_2O_3	34 kev	1.006	6.307
B_2O_3	thick	1.006	6.313
B	thick	1.006	6.281
	Average of Q = 8.574 ± 0.014 Mev.		

(4) $C^{13}(d,\alpha)B^{11}$, (5) $C^{13}(d,\alpha)B^{11*}$, (6) $C^{13}(d,t)C^{12}$ and (7) $C^{13}(d,p)C^{14}$

The disintegration of C^{13} by deuterons gives rise to several kinds of particles. The emitted particles, identified by their e/m ratio, pulse size in the scintillation counter, and the relative spread of energy of emitted particles in the target, corresponded to the above reactions.

The targets were prepared by John D. Seagrave by depositing C^{13} on thin tantalum strips by heating them in an atmosphere of CH_3I vapour, enriched to 61% C^{13}. The thickness of the carbon layers, estimated from the energy spread of the outgoing particles, was approximately 50 kev for normally incident deuterons of 1 Mev. The deuteron beam of 1.006 Mev from the Van de Graaf generator was used. Magnetic analysis of the elastically scattered deuterons showed surface contamination layers to be negligibly small. From previous experience of this laboratory the surface contamination was assumed to be of the order of 0.2 kev for 1 Mev protons at normal incidence, and corresponding small

corrections were made.

For reaction (4), five thick targets and one thin target were used. The energy of the emitted alpha particles from these different targets was distributed randomly within 10 kev. The average was 4.399 Mev, giving $Q_4 = 5.164 \pm 0.006$ Mev. From two thick target measurements which agree to one kev, we obtained $Q_6 = 1.310 \pm 0.003$ Mev. The error is very small. From two thin targets and one thick target which agree to within 4 kev in the alpha particle energy, we obtained for reaction (7), $Q_7 = 5.940 \pm 0.004$ Mev. The error is again very small. a pronounced peak of $C^{12}(d,p)C^{13}$ was noticed, roughly at $Q = 2.711 \pm 0.03$ Mev.

Relativistic corrections and corrections for the nonlinearity of the field measurement were made as in the other Q measurements. Due to the triple mass of the tritons, their momentum/charge ratio with the bombarding energy at 1 Mev is very close to that of the Po alphas for calibration and no correction of the non-linearity of field measurement was needed. The probable errors in all these measurements include statistical errors as well as all known systematic srrors, one of the most significant being the 0.2^{o} uncertainty in the angle of observation. Table III gives the detailed analysis of the errors of the Q measurements. The statistical error in the average of Q from the two different ways (see section on $Li^{7}(p,\alpha)He^{4}$) agrees in each of these cases.

Our values are in good agreement with those obtained recently by Bechner and his collaborators: $Q_4 = 5.160 \pm 0.010$ Mev, $Q_6 = 1.310 \pm 0.006$ Mev, and $Q_7 = 5.948 \pm 0.008$ Mev; also with Curling and Newton's value (Table IV). The agreement between independent measurements of the $C^{13}(d,\alpha)B^{11}$ Q value is particularly fortunate, since this reaction is

of critical importance in determining the mass of the nuclei lighter than B^{11} in terms of O^{16}. The only common observational factors in the two measurements are the absolute voltage scale for calibration of the bombarding energy and the Po alpha energy for calibration of the fluxmeter, used by both investigators.

From the experimental values of $C^{12}(d,p)C^{13}$ and $H^2(d,p)H^3$ the value of Q_6 can be calculated. The result is 1.308 ± 0.007 from the Q values listed in Table IV, in good agreement with the direct measurements.

In addition to the ground state transitions, a group of alpha particles was observed which we have tentatively identified with the reaction $C^{13}(d,\alpha)B^{11*}$ leaving B^{11} excited by 2.107 ± 0.017 Mev above the ground state. The existence of this lowest excited state in B^{11} has been recently reported by Bateson[21] with an excitation of 2.15 ± 0.06 Mev and by Buechner and Van Patter with 2.141 Mev[22] from study of the $B^{10}(d,p)B^{11}$ protons, besides the earlier values of 2.14 ± 0.06 Mev[23,24] and 1.92 ± 0.2 Mev[25].

Following the procedure of obtaining nuclear reaction cross sections from thick target spectra given by Snyder et al.[1], we found for 990 kev deuterons a differential cross section at 90° of 7 mb/steradian for reaction (4) and 2 mb/steradian for reaction (6). The high energy protons from reaction (7) were able to pass completely through the ZnS phosphor screen of the scintillation counter, producing a non-uniform pulse height distribution and making the counter efficiency uncertain (the bias used was 5 volts), so that we are not able to give a value for this cross section.

The rough plot in Fig. 11 shows the relative intensities of the reactions, including the pronounced $C^{12}(d,p)C^{13}$ peak. Following is a summary of the individual measurements.

Bombarding energy = 1.006 Mev, $\theta = 89.3^{\circ}$

Reaction	Target thickness	E_2 (Mev)	Average Q (Mev)
$C^{13}(d,\alpha)B^{11}$	thick	4.404	5.164 ± 0.006
	thick	4.402	
	thick	4.398	
	thick	4.400	
	thick	4.397	
	57 kev	4.394	
$C^{13}(d,t)C^{12}$	thick	1.720	1.310 ± 0.003
	thick	1.721	
$C^{13}(d,p)C^{12}$	thick	6.348	5.940 ± 0.004
	65 kev	6.348	
	65 kev	6.352	

(8) $N^{15}(p,\alpha)C^{12}$

Potassium nitrate (KNO_3) enriched to 61% of N^{15} with 39% of N^{14} was evaporated from the furnace on to target backing made of copper foil. This compound melts at rather low temperature and is known to decompose around 400°C. The evaporation proceeded as the tantalum

furnace became barely dull red in darkness, possibly accompanied by decomposition of the material. It is difficult to control the target thickness, but after many trials, several good targets were obtained. Two measurements have been made, one with a thick target and one with a thin target, the latter having a thickness of 18 kev for the outgoing alpha particles as calculated from the thick target yield. A bombarding energy of 1.036 Mev was chosen in view of the resonance at 1.015 Mev with a half width of 0.16 Mev[26]. The thick target curve was corrected for the variation of cross section. The thick and the thin target measurements gave the same result, the energy of the emitted alpha particles being 4.438 Mev in both cases; the average of Q is Q_8 = 4.961 ± 0.006 Mev. Freeman's value is 4.96 ± 0.05 Mev[27] and Buechner's is 4.960 ± 0.007 Mev (Table IV). The value calculated from the experimental values of $C^{12}(d,p)C^{13}$ and $N^{15}(d,\alpha)C^{13}$ listed in Table IV is 4.958 ± 0.010 Mev.

(9) $O^{16}(d,\alpha)N^{14}$

A number of compounds containing oxygen can be used for target material. We have used four of them: (1) thin SiO_2 film obtained by blowing a bit of quartz to form a bubble. Evaporation of SiO_2 from the furnace is possible but no measurement had been made. (2) litharge (lead monoxide) evaporated on to backing of silver leaf. This compound melts at 888 degrees Centigrade. Good targets were easy to obtain; we found it to be satisfactory to work with. (3) copper oxide (CuO) obtained by heating a copper foil over a flame and oxidizing it. (4) potassium nitrate on tantalum target prepared as described above on the reaction $N^{15}(p,\alpha)C^{12}$. No surface contamination layer has

been observed on any of the above freshly prepared targets and corrections are considered to be negligible.

The reaction cross section of this reaction falls continuously with the bombarding energy, a common occurrence in these reactions. For the thick target curve the energy of the alpha particles coming from the front surface of target was taken by extrapolation from the slowly-sloping plateau part on the lower energies of the thick target curve, and was about 5% higher than the half height point of the curve. The thin target peaks were corrected in the usual way by comparing the counts with the thick target yield. The thick target yields for PbO and CuO were calculated from the stopping powers and the experimental thick target yield of SiO_2. The four measurements, two thick targets and two thin targets, as given b elow, agree to within 6 kev. The average of Q_9 is $Q_9 = 3.119 \pm 0.005$ Mev, in agreement with a recently published value of 3.112 ± 0.006 Mev by Strait, Van Patter, Buechner and Sperduto (Table IV) using magnetic analysis.

This reaction forms the first link between O^{16} and the lighter nuclei. It is essential in establishing accurate values of the masses of light nuclei from nuclear disintegration data.

The competing reaction $O^{16}(d,p)O^{17}$ was noticed and appeared to be about half as intense as the reaction $O^{16}(d,\alpha)N^{14}$. No accurate measurement of the Q value was made.

The following is the summary of the individual Q values measured.

Bombarding energy = 1.006 Mev, $\theta = 89.3^{\circ}$

Target material	Target thickness	E_2 (Mev)
SiO_2	thick	3.105
KNO_3	thick	3.104
PbO	13 kev	3.099
CuO	13 kev	3.100
	Average of Q = 3.119 ± 0.005 Mev.	

Table II. Reaction Energies Determined by the 16" Magnetic Spectrograph (1950)

Reaction	The present determination (Mev)	Other determinations (Mev)
$Li^7(p,\alpha)He^4$	17.338 ± 0.011	17.340 ± 0.014 *
		17.28 ± 0.03 #
$Be^9(d,\alpha)Li^7$	7.151 ± 0.010	7.150 ± 0.008 *
$B^{11}(p,\alpha)Be^8$	8.574 ± 0.014	8.567 ± 0.011 *
		8.60 ± 0.10 &
$C^{13}(d,\alpha)B^{11}$	5.164 ± 0.006	5.160 ± 0.010 *
$C^{13}(d,t)C^{12}$	1.310 ± 0.003	1.310 ± 0.006 *
$C^{13}(d,p)C^{14}$	5.940 ± 0.004	5.948 ± 0.008 *
$N^{15}(p,\alpha)C^{12}$	4.961 ± 0.006	4.960 ± 0.007 *
		4.96 ± 0.05 %
$O^{16}(d,\alpha)N^{14}$	3.119 ± 0.005	3.112 ± 0.006 *

* Strait, Van Patter, Buechner and Sperduto, Phys. Rev. 81, 747 (1951).

Smith, Phys. Rev. 56, 548 (1939).

& Oliphant, Kempton, and Rutherford, Proc. Roy. Soc. (London) A150, 241 (1935).

% Freeman, Proc. Roy. Soc. (London) 63A, 668 (1950).

Table III. Errors of the Reaction Energies

	Cause	Statistical	Systematic
E_1:	electrostatic analyzer	$\delta E/E = 0.1\%$	$\delta E/E = 0.1\%$
	surface loss	100% of the assumed surface layer	100% of the assumed surface layer
θ:			0.2^{o}
E_2:	energy of ThC' or Po alphas		2 kev in ThC' or 1 kev in Po alphas
	relative displacement between the calibration source and the beam spot		0.010"
	fluxmeter reading	1/7000	
	nonlinearity correction		10% to 20% of the correction
	surface loss	100% of the assumed surface layer	100% of the assumed surface loss
	location of E_2 on the curve (graph error)	$\frac{1}{\sqrt{2}}$ of the possible error due to the uncertainty in drawing the right curve through the experimental points	same as left

PART IV

THE MASSES OF LIGHT NUCLEI

Introduction.

The accurate determination of nuclear masses is a primary problem in nuclear physics. Mass spectrographic measurements in comparison with nuclear reaction energy data make it possible to test and confirm experimentally the equivalence of mass and energy, $E = Mc^2$, one of the cornerstones of modern physics. From the established equivalence of mass and energy there follow many consequences of interest. A determination of the energy release in a nuclear reaction is a measure of the mass difference between the reacting nuclei and their products. The mass defects or binding energies of nuclei can be calculated from the accurately determined masses, assuming their constituents. This result permits us to reach important conclusions concerning the structure of nuclei and the forces acting among their constituents. In these theoretical considerations the masses of the lightest nuclei, n, H^1, H^2, H^3, He^3 and He^4 have been of particular interest. Among other applications of accurate masses are the experimental determination of range-energy relations for ionizing particles in different media, the interpretation of molecular band spectra, and the determination of chemical atomic weight scale.

Methods of Determining Nuclear Masses.

There are many methods, rough or accurate, physical or chemical, for determining the masses of different nuclei in their atomic,

ionic or nuclear form. Since the mass of the electron and the binding energy of electrons in an atom is sufficiently accurately known, we need not distinguish among the three terms except as to the numerical values. In the following, we will use the term nuclear mass freely, but for all numerical values, as those listed in the tables, we will always use atomic masses of the nuclides, unless otherwise indicated.

The chief methods of the accurate determination of masses are: first, mass spectroscopy, essentially for ionic masses, and secondly, nuclear reaction energy measurements, essentially for nuclear masses. Mass spectrographs give direct measurements of masses and up to the recent time have served to determine the main mass scale. Nuclear reaction energy values have been used chiefly to provide a check of the mass spectroscopic data and to deduce the masses of radioactive nuclei and of nuclei too rare to be measured in the mass spectrograph[23]. Until recently it was not possible to determine any substantial portion of the mass scale from nuclear data alone. The present work is a first trial for such a determination, as a natural consequence of the work of Tollestrup, Fowler and Lauritsen[28]. Another well known method is the use of isotopic effect on the molecular band spectrum. The stable isotopes of carbon, nitrogen and oxygen were discovered by this method (1929-31); and the first precise determination of the mass of deuteron employed this effect (1932); and the method has been developed further with the recent microwave techniques. In a few cases, accuracy has been comparable to that given by the mass spectroscopy and nuclear data, but as there is yet not enough data from that method, we will not include it in further discussion.

NUCLEAR MASSES FROM DISINTEGRATION ENERGY DATA

Experimental Values of Nuclear Reaction Energies.

The recent accumulation of accurately determined Q-values from nuclear reactions makes it possible to derive the masses of light nuclei from these nuclear values exclusively, using the law of conservation of mass-energy and Einstein's relation $E = Mc^2$. Of course, a first approximation value of masses derived from mass spectrography or other methods is necessary beforehand for the establishment of the more accurate Q-values from experimental measurements.

As many of the nuclear reactions form cycles, the number of measured Q-values is larger than the number of masses to be evaluated; thus the data are overdetermined. To obtain numerically consistent values of masses, some kind of adjustment of the experimental Q values has to be made(28). Least-squares adjustment is possible and the result significant in the sense that the required amounts of adjustment are well within the experimental errors of the Q values. In this manner, a mass table for light nuclei from n to F^{20} has been derived from nuclear data, with O^{16} = 16.000 000 as the standard (Table IV).

The experimental Q values used in deriving the masses are listed in the second column of Table IV with a reference to the source of each item in the last column. Only those measurements with the smallest probable errors have been included. In most of these measurements, electrostatic and magnetic deflection for incident beams and emitted particles (electrons, heavy particles or pairs produced by gammas) have been employed to determine the energy of the bombarding

particles and emitted particles. In some cases, reaction thresholds or radiative capture of thermal neutrons have been involved. Measurements depending on total ionization have been included. Ordinary range measurements and photographic emulsion measurements have not been included because of their relatively large uncertainties, from both experimental errors and the empirical range-energy relations.

Regarding the reported errors of the measurements, 30 kev has been used as a reference point in choosing the data, and 15 kev as another reference point. Measurements with errors larger than 30 kev were not included. The Q values chosen range from about 18 kev for $H^3(\beta^-)He^3$ to about 17 Mev for $Li^7(p,\alpha)He^4$. The reported errors are from 0.2 kev up and are all within 15 kev except five cases in which the measurements have errors ranging up to 30 kev but smaller than 1% of the respective Q values. The latter ones are included for completeness and contribute a negligible amount to the average Q values. The errors of most of the measurements are much better than 1% except those with Q values below 1 Mev.

Because of the procedure of weighting the data, the inclusion of additional data with larger errors would have a negligible effect on the average values used. But it should be mentioned that the calculation of nuclear masses from Q values is a linear and additive operation, and consequently, absolute errors of the Q values and not their percentage errors are important in the final stages of calculation. Hence, a low energy reaction should not be excluded simply because of the large percentage error of its measured Q value.

For the successive measurements on the same reaction from the same laboratory, only the most recent value has been used. Notable

examples are the threshold determinations by the Wisconsin group. Hanson and Benedict's values[29] were replaced by that of Herb, Snowdon and Sala[17], etc.

Several measurements have been omitted even though a small error was claimed. In the original data collected for the present purpose these values appeared to be dubious by the large inconsistency of each value with other similar determinations or by other tests described below, and it happened that each of these values has been shown or is believed to be incorrect due to some experimental mistakes; therefore, they are omitted from the present calculation. An inaccurate value with a correspondingly large error would have negligible effect on the average value but an inaccurate value with a small reported error would unduly shift the average if the values were weighed according to the reported errors in taking the average.

The indication that an experimental Q value may not be right was obtained by comparing the different measurements of the same reaction. One value might seem to be inconsistent with other values or with the mean value. In the determination of consistency, Birge's criterion[30] of external consistency against internal consistency has been used. There are several tests or definitions proposed by different authors for consistency of observed values.* Some are more arbitrary than others, but due to the statistical nature of the problem, all these definition may be regarded to have similar significance, useful

---

* See, for example, Worthing and Geffner, Treatment of Experimental Data, John Wiley & Sons, New York (1943), p. 198.

for detecting inconsistencies in different observed values of the same physical quantity. It also should be noted that only values with reported errors can be treated by these criteria. Usually, when two values differ by as much as twice of the sum of the two errors, they may be regarded as inconsistent. As physicists often show individual tendencies in assigning errors to experimental results -- some assigning too large an error -- non-overlapping of errors of two values or between one value and the mean of several values require careful examination.

Another check was provided by comparing certain fundamental mass difference, derived from a nuclear cycle containing the Q value in question, with the values of the same mass difference derived from other nuclear cycles. For example, both of the experimental values for the $C^{11}(\beta^+)B^{11}$: $\beta^+ = 0.981 \pm 0.005$ Mev(31) and 0.993 ± 0.010 Mev(32) are inconsistent with the $n - H^1$ mass difference and the $B^{11}(p,n)C^{11}$ threshold(33) which is thought to be more accurate than the beta spectrum end-point. The meaning of the word "inconsistency" here is similar to that given in the last paragraph. More will be said about the nuclear cycles and the fundamental mass differences in the following sections.

As the history of the e/m values demonstrates, one should not rely upon any of the above-mentioned criteria or tests to make final decisions and therefore lead to a false man-made internally consistent system. Especially since usually only a few values are involved, we have here a case of extreme small-sampling where statistical fluctuation may be quite large apparently. Further examination to the experimental value is necessary after it has been shown to be dubious by these tests, and it may be discarded only when we have some other

reason to believe that is is in error. As a result of the choice of data, no value listed in Table IV differs from other values of the same Q or from the mean value of the Q by as much as twice the sum of two errors concerned. The following is a list of Q values which have small reported errors but have not been included in the present calculation.

Reaction	Q (Mev)	Reference
$H^2(\gamma,n)H^1$	- 2.181 ± 0.005	Meyer, Zeits. f. Physik 126, 336 (1949).
	- 2.189 ± 0.007	Kimura, Mem. Coll. Sci. Kyoto Imp. Univ. 22, 237 (1939).
	- 2.183 ± 0.02	Myers and Van Atta, Phys. Rev. 61, 19 (1942).
	- 2.185 ± 0.02	Widenbeck and Marhoefer, Phys. Rev. 67, 54 (1945).
$H^2(d,n)He^3$	3.30 ± 0.01	Argo, Phys. Rev. 74, 1293 (1948).
$Be^9(\gamma,n)Be^8$	- 1.637 ± 0.010	Myers and Van Atta, Phys. Rev. 61, 19 (1942).
	- 1.630 ± 0.006	Widenbeck and Marhoefer, Phys. Rev. 67, 54 (1945).
$Be^9(p,d)Be^8$	0.547 ± 0.006	Allison, Skaggs, and Smith, Phys. Rev. 57, 550 (1940).
	0.541 ± 0.003	Rosario, Phys. Rev. 74, 304 (1948).
$C^{11}(\beta^+)B^{11}$	β^+= 0.981 ± 0.005	Townsend, Proc. Roy. Soc. 177, 357 (1940-41).
	β^+= 0.993 ± 0.01	Siegbahn and Bohr, Arkiv. f. Astron. Math. Fysik 30B, No. 3 (1944).
$N^{13}(\beta^+)C^{13}$	β^+= 1.218 ± 0.004	Townsend, Proc. Roy. Soc. 177, 357 (1940-41).
	β^+= 1.24 ± 0.02	Siegbahn and Slätis, Arkiv. f. Astron. Math. Fysik 32A, No. 9 (1945).

Also the following values were not included, the reported errors of these values were 30 kev.

$Be^9(p,\alpha)Li^6$	2.074 ± 0.03 Mev	Rosario, Phys. Rev. 74, 304 (1948).
$N^{13}(\beta^+)C^{13}$	β^+ - 1.25 ± 0.03	Cook, Langer, Price and Sampson, Phys. Rev. 74, 502 (1948).
$F^{19}(n,\gamma)F^{20}$	6.63 ± 0.03	Kinsey, Bartholomew and Walker, Phys. Rev. 78, 481 (1950).

As accurate values of the thresholds $H^2(\gamma,n)H^1$ and $Be^9(\gamma,n)Be^8$ have been available, measurements on the ratio of these two thresholds were not included to avoid increasing complexity that would be introduced into the manipulation of the data. They are:

1.342 ± 0.006	Myers and Van Atta (see above).
1.340 ± 0.003	Widenbeck and Marhoefer (see above).
1.338 ± 0.004	Waldman and Miller, Phys. Rev. 74, 1225 (1948).
1.35 ± 0.03	McElhinney, Hanson, Becker, Duffield and Diven, Phys. Rev. 75, 542 (1949).

Corrections to the experimental value:

Standards or fundamental constants used in an experimental calculation change continuously with time. Many Q measurements have used some older values of, for instance, ThC" gamma ray energy, $Li^7(p,n)Be^7$ threshold, faraday, conversion factor between mass and energy, etc. Corrections should be made to conform to recent values, but a complete revision of this kind has not been undertaken in the present calculation. In a few cases which happened to be noticed, the correction has been made in the way given by the respective footnote in Table IV.

As the result of the choice of data, the Q values used in the present calculation have all been done in the last few years with the exception of Lyman's value of the maximum energy of positrons from N^{13} decay which was published in 1939.

The Average of Measurements Belonged to the Same Q.

For those Q values which have been measured by more than one investigator, the several measurements have been averaged together by weight, equal to the inverse square of the respective error. Inverse reactions or reactions giving the same Q value have been averaged together too, by weight. An example is items 2, 3 and 4 of Table IV: $H^1(n,\gamma)H^2$, $H^2(\gamma,n)H^1$ and $H^2(p,n)2H^1$ all giving the binding energy of deuteron. The mean values are listed in column 3 of Table IV and are used as the experimental Q values in subsequent calculations.

Explicitly, the weighted mean of several measurements belonging to the same Q value is

$$\bar{Q} = \frac{\sum_i w_i Q_i}{\sum_i w_i} = \frac{\sum_i \frac{1}{p_i^2} Q_i}{\sum_i \frac{1}{p_i^2}}, \qquad (4\text{-}1)$$

where Q_i is one of the measurements, p_i is its probable error, and $w_i = 1/p_i^2$ its weight in taking the mean. There are two ways of giving $\bar{p}$, the error of the mean value. The first is by internal consistency, namely,

$$\frac{1}{\bar{p}^2} = \sum_i \frac{1}{p_i^2}. \qquad (4\text{-}2)$$

The second is by external consistency, namely,

$$\bar{p} = 0.67\sqrt{\frac{\sum_i w_i (Q_i - \bar{Q})^2}{(n-1)\sum_i w_i}}. \qquad (4\text{-}3)$$

where n is the number of measurements. For consistent measurements of the same Q, the expression (4-2) has been used. For inconsistent measurements of the same Q, that is, for which the $\bar{p}$ calculated from external consistency (4-3) is substantially greater than the $\bar{p}$ calcu-

lated from internal consistency (4-2), the $\bar{p}$ from (4-3) has been used. The only examples are items 22 and 36 in Table IV.

The published errors have been assumed, for lack of better alternatives, in every case to be a reliable reflection of the real accuracy of the experimental value. They have all been regarded as the conventional 50% probability "probable error".

Nuclear Cycles and Their Usefulness.

Fig. 12 gives a view of the Q values used in deriving the masses. The 53 Q values can be divided into three groups: (A) those interlinking nuclei below the standard or fixed point O^{16}, (B) those above O^{16}, and (C) the dotted lines in Fig. 12, leading to nuclei which can be approached, at present, by no other reaction whose Q value is accurately known. At present, there is little connection between the groups (A) and (B). Group (A) contains 40 Q values and 20 masses to be determined, besides the standard O^{16}.

Many nuclear cycles can be formed by the combination of suitable reactions. They are useful in that: (1) they give the best experimental values of certain fundamental mass differences; (2) these fundamental mass differences can serve as tests of internal consistency of the nuclear data; and (3) they can be used to make regional least-squares adjustment of the experimental Q values and thereby to obtain the values of masses which are numerically consistent and presumably with some improved precision. The improvement in precision is a possible result of the adjustment of overdetermined but statistically consistent data.

Table V shows all the independent and simplest nuclear cycles, in addition to the three direct determinations: $n(\beta^-)H^1$, $H^1(n,\gamma)H^2$ and $H^2(d,p)H^3$. The cycles fall into five groups, giving, respectively: (1) zero; (2) $n - H^1$; (3) $n + H^1 - H^2$; (4) $2H^2 - H^1 - H^3$; and (5) $2H^2 - He^4$.

In Table V there are 21 cycles below O^{16}. A new Q value, $2H^2 - He^4$, which so far has not been experimentally observed, is involved. This makes the number of independent cycles check with the number of Q values and unknown masses in group (A) given above. Above O^{16}, there are two cycles, one giving the sum zero, another giving $n - H^1$.

The first choice of the independent set of cycles is arbitrary, but the cycles that can subsequently be constructed out of the first ones by linear combinations should not be included in the calculation because of statistical reasons. For, otherwise, we would be able to decrease the probable error of the mean values of the fundamental mass differences indefinitely by going round and round. For purpose of reference, we can construct a cycle giving $n - H^1$ by adding a cycle giving zero to another giving $n - H^1$. A cycle giving $n + H^1 - H^2$ and a cycle giving zero would give another cycle of $n + H^1 - H^2$. $n - H^1$ and $n + H^1 - H^2$ would give $2H^1 - H^2$. Also, two $n - H^1$ cycles would give a zero, etc.

A fundamental mass difference was obtained from each cycle by combining suitably the experimental Q values in the cycle, the errors combining by squares. Weighted mean of a fundamental mass difference from the different values of the same mass difference from different cycles was obtained, weighting inversely as the square of the error as before. Direct determinations were included, equivalent to one cycle in each case. For example, $n(\beta^-)H^1$ is the first item in

the group giving n - H^1 in Table V. The weighted mean values of the four fundamental mass differences are assumed to be the most probable values that are available from our present experimental knowledge. The probable error of each weighted mean is an indication of how good a value we have for that fundamental mass difference.

There are five cycles in Table V, each of which should give a sum of zero. Four belong to group (A) and one belongs to group (B). The deviation of the experimental sum from zero ranges from 2 to 15 kev, all within the respective error of the sum.

The weighted mean of n - H from the eight items is 782.4 kev. The probable error from internal consistency is p_i = 0.93 kev. The probable error from external consistency is p_e = 0.23 kev. Birge's test gives p_e/p_i = 0.25. Taking out the second item which swamps the statistics, we have for the weighted mean of n - H^1 from the remaining 7 cycles, 782.7 kev, and p_i = 2.6 kev, p_e = 0.72 kev, p_e/p_i = 0.27. The arithmetic average of the eight values is 784.0 kev. Leaving out the fifth item, the arithmetic average becomes 782.3 kev. A closer look at the data shows that the weighted mean is mainly determined by the cycles 2, 3 and 4 and the threshold measurements in these three cycles were all calibrated against the $Li^7(p,n)$ threshold 1.882 ± 0.002 Mev. In view of this correlation of data, the probable error of the weighted mean of n - H^1 has been set at 1 kev.

The fundamental difference n + H^1 - H^2 is given by six items in Table V. The weighted mean is 2.225 Mev, p_i = 1.9 kev, p_e = 1.3 kev, and p_e/p_i = 0.68. The arithmetic average of the six items is 2.219 Mev. The probable error of the weighted mean has been set at 2 Kev.

The fundamental mass difference $2H^2 - H^1 - H^3$ is given by three items in Table V. The weighted mean and the probable error p_i is 4.032 ± 0.004 Mev.

In the four cycles listed for the fundamental mass difference $2H^2 - He^4$, the first two give it directly, the last two have to be combined with $n + H^1 - H^2$. The weighted mean of $n + H^1 - H^2$ above, 2.225 ± 0.002 Mev, has been used. The weighted mean of $2H^2 - He^4$ and the probable error p_i is 23.832 ± 0.007 Mev. To see that the last item in this group consists of a cycle in Fig. 12, connect He^4 and H^2 by the reaction $He^4(d,\alpha)H^2$ which is simply the scattering of deuterons from He^4 with a Q value of zero.

The internal consistency of the nuclear data is evident from these cycles. For the reactions of group (A), each reaction except $O^{16}(d,\alpha)N^{14}$ and $C^{13}(d,\alpha)B^{11}$ is involved in at least one cycle, and each cycle is a check of consistency.

Masses of the Group (A).

This group contains 40 Q values and 20 unknown masses. Since the experimental Q values have been shown to be statistically consistent (except the two reactions $O^{16}(d,\alpha)N^{14}$ and $C^{13}(d,\alpha)B^{11}$ for which there is no internal test of consistency), we can find the most probable values of the masses, as well as a numerically consistent set of Q values and the probable errors of these adjusted values, by overall least-squares procedure. This will involve matrices of the 20th order and can be carried out with an electronic computer.

Two assumptions, or approximations, have been made in considering the use of a least-squares procedure, besides the fundamental

assumption that all uncertainties in nuclear experiments follow the normal distribution. The first is that all the published errors are probable errors. The second is that the experimental Q values are observationally independent of each other.

Least-squares adjustment has been treated in many standard works*. Let the "observation equations" connecting the k masses and n Q values ($n \geq k$) be

$$\begin{aligned}
a_{11} M_1 + a_{12} M_2 + \cdots + a_{1k} M_k &= Q_1 + \Delta_1, \quad w_1 = \frac{1}{p_1^2} \\
a_{21} M_1 + a_{22} M_2 + \cdots + a_{2k} M_k &= Q_2 + \Delta_2, \quad w_2 = \frac{1}{p_2^2} \\
&\vdots \\
a_{n1} M_1 + a_{n2} M_2 + \cdots + a_{nk} M_k &= Q_n + \Delta_n, \quad w_n = \frac{1}{p_n^2}.
\end{aligned}$$

Here $a_{11}, \ldots a_{nk}$ are the constant coefficients, usually 1, - 1 or 0. $M_1, \ldots M_k$ are the unknown masses; $Q_1, \ldots Q_n$, the experimental Q values; $\Delta_1, \ldots \Delta_n$, the adjustments necessary for numerical consistency; $p_1, \ldots p_n$, the probable errors of the experimental Q values; and $w_1, \ldots w_n$, the corresponding weights. Following the principle of least-squares, we assume that the maximum probability of occurrence of the observed set, i.e., the experimental set, of Q values requires that

$$\sum_{j=1}^{n} w_j \Delta_j^2 = \text{minimum.}$$

Since the M's are the independent variables, it follows that

---

* For example: Deming, W. E., "Statistical Adjustment of Data", John Wiley & Sons, New York (1943); Worthing, A. G. and Geffner, J., "Treatment of Experimental Data", John Wiley & Sons, New York (1943).

$$\frac{\partial(\Sigma w_j \Delta_j^2)}{\partial M_1} = \frac{\partial(\Sigma w_j \Delta_j^2)}{\partial M_2} = \cdots = \frac{\partial(\Sigma w_j \Delta_j^2)}{\partial M_k} = 0 .$$

Rewrite the observation equations as

$$\begin{aligned} a_{11} M_1 + R_1 &= \Delta_1 \\ a_{21} M_1 + R_2 &= \Delta_2 \\ &\vdots \\ a_{n1} M_1 + R_n &= \Delta_n . \end{aligned}$$

We have

$$\frac{\partial(\Sigma w_j \Delta_j^2)}{\partial M_1} = \frac{\partial}{\partial M_1}\left\{ M_1^2(\Sigma w_j a_{j1}^2) + 2M_1(\Sigma w_j a_{j1} R_j) + \Sigma w_j R_j^2 \right\}$$

$$= 2\left\{ M_1(\Sigma w_j a_{j1}^2) + \Sigma w_j a_{j1} R_j \right\} = 0 .$$

etc.

Or,

$$\begin{aligned} (\Sigma w_j a_{j1}^2) M_1 + (\Sigma w_j a_{j1} a_{j2}) M_2 + \cdots + (\Sigma w_j a_{j1} a_{jk}) M_k &= 0 \\ (\Sigma w_j a_{j2} a_{j1}) M_1 + (\Sigma w_j a_{j2}^2) M_2 + \cdots + (\Sigma w_j a_{j2} a_{jk}) M_k &= 0 \\ \vdots \qquad\qquad \vdots \qquad\qquad & \vdots \\ (\Sigma w_j a_{jk} a_{j1}) M_1 + (\Sigma w_j a_{jk} a_{j2}) M_2 + \cdots + (\Sigma w_j a_{jk}^2) M_k &= 0 . \end{aligned}$$

These are the "normal equations", k in number.

In terms of matrices, we have

$$\underset{\sim}{A} = \begin{pmatrix} a_{11} & a_{12} & \cdots & a_{1k} \\ a_{21} & a_{22} & \cdots & a_{2k} \\ & & & \\ a_{n1} & a_{n2} & \cdots & a_{nk} \end{pmatrix} ,$$

$$\underline{M} = \begin{pmatrix} M_1 \\ M_2 \\ \vdots \\ M_k \end{pmatrix}, \qquad \underline{Q} = \begin{pmatrix} Q_1 \\ Q_2 \\ \vdots \\ Q_n \end{pmatrix},$$

$$\underset{\sim}{p^2} = \begin{pmatrix} p_1^2 & 0 & 0 & \cdots \\ 0 & p_2^2 & 0 & \cdots \\ \vdots & \vdots & \vdots & \\ 0 & 0 & \cdots & p_n^2 \end{pmatrix},$$

$$\underset{\sim}{w} = (\underset{\sim}{p^2})^{-1} = \begin{pmatrix} \frac{1}{p_1^2} & 0 & 0 & \cdots \\ 0 & \frac{1}{p_2^2} & 0 & \cdots \\ \vdots & \vdots & \vdots & \\ 0 & 0 & \cdots & \frac{1}{p_n^2} \end{pmatrix}.$$

The observation equations becomes

$$\underset{\sim}{A}\,\underline{M} = \underline{Q} .$$

The normal equations are

$$\underset{\sim}{A}^* \underset{\sim}{w}\,\underset{\sim}{A}\,\underline{M} = \underset{\sim}{A}^* \underset{\sim}{w}\,\underline{Q} ,$$

where $\underset{\sim}{A}^*$ is the transposed matrix of $\underset{\sim}{A}$, or $A^*_{ji} = A_{ij}$.

Multiplying both side by $(\underset{\sim}{A}^* \underset{\sim}{w}\,\underset{\sim}{A})^{-1}$, we have

$$\underline{M} = (\underset{\sim}{A}^* \underset{\sim}{w}\,\underset{\sim}{A})^{-1}\,\underset{\sim}{A}^* \underset{\sim}{w}\,\underline{Q} ,$$

giving the most probable values of masses in terms of experimental Q values.

Writing out the components of the matrix $\underline{M}$, we have

$$M_i = \alpha_{i1} Q_1 + \alpha_{i2} Q_2 + \cdots + \alpha_{in} Q_n , \quad i = 1, 2, \ldots k .$$

The probable errors of the M's are

$$\sqrt{\alpha_{i1}^2 p_1^2 + \alpha_{i2} p_2^2 + \cdots + \alpha_{in} p_n^2} \quad .$$

The adjusted Q values, Q', can be calculated from these adjusted values of M from the observation equations, but the probable errors of the adjusted values Q' should not be calculated as though the M's are observationally independent of each other. Because the adjusted M's depend on the experimental Q values, they are not longer observationally independent of each other. They are mutually correlated because of the adjustment. It can be shown(34) that the square of the the square of the probable error of the adjusted value Q_j' is given by the diagonal element of a matrix,

$$(p_j')^2 = \{ \underset{\sim}{A} (\underset{\sim}{A}^* \underset{\sim}{w} \underset{\sim}{A})^{-1} \underset{\sim}{A}^* \}_{jj} \quad .$$

Because of the large number of independent parameters involved in an overall adjustment of the 40 Q values and the necessity of recalculating the whole set each time a new experimental value of Q is added, a regional least-squares adjustment has been made. In view of the uncertainties introduced by the two basic assumptions mentioned before and the unadjustability of the two key reactions $C^{13}(d,\alpha)B^{11}$ and $O^{16}(d,\alpha)N^{14}$, it seems that this partial or regional adjustment, essentially an approximation to the overall adjustment, has given mass values with similar significance as that given by an overall adjustment. As new Q values become available, the now overall adjustment will become a regional adjustment again. There is no reason to believe that, apart from quantitative difference, there is any essential distinction in the statistical behaviour of the two ways of adjustment. The result is also justified by the fact that the difference between the

adjusted value and the experimental value of a Q is, practically in every case, less than its experimental error; most of the amounts of adjustment being only a fraction of the respective experimental probable errors (Table IVa).

In this procedure, the nuclear cycles and the weighted mean of the fundamental mass differences were used. The Q values in each cycle were adjusted to make their sum numerically equal to the weighted mean of the fundamental mass difference. Now the weighted sum of the square of require amounts of adjustment $\sum_j w_j \Delta_j^2$ to be minimized is summed over the reactions included in one cycle, instead of over the 40 reactions as in the overall adjustment. The auxiliary condition is that the algebraic sum of the reactions in the cycle should give the weighted mean of the fundamental mass difference. Minimizing of the sum $\sum_j w_j \Delta_j^2$ leads to the rule that the discrepancy between the experimental sum of the Q's in a cycle and the weighted mean of the fundamental mass difference should be divided among the several reactions included in that cycle, inversely proportional to the weight of each Q or directly proportional to the square of the experimental probable error. The probable error in the adjusted Q value is a function of the experimental probable errors of the reactions in the cycle as well as the error in the mean value of the mass difference to which the cycle has been fitted. It can be shown that p_i^*, the probable error in Q_i^*, the adjusted value of Q_i is given by

$$(p_i^*)^2 = p_i^2 \left\{ 1 - \frac{p_i^2}{\sum_j p_j^2} + \frac{p_i^2}{\sum_j p_j^2} \cdot \frac{p_C^2}{\sum_j p_j^2} \right\},$$

where p_i is the probable error of the experimental Q_i, p_2, the probable error of the experimental Q_2, etc., and p_C, the probable error in the weighted mean of the fundamental mass difference. p_C is zero for a "zero" cycle, and negligible in n - H^1 and n + H^1 - H^2 cycles.

Due to the weighting procedure, an experimental Q value with a 1 or 2 kev probable error is practically unaffected by the adjustment. Certain Q values happen to belong to more than one cycle. Then the adjusted values of the same Q from different cycles may be the same or may be different. Table IVb gives all the cases of these coincidences and discrepancies. When three or four reactions are involved in two cycles having one reaction in common, we can minimize the sum $\sum_j w_j \cdot \Delta_j^2$ over them, using two auxiliary conditions. The required adjustments can be found easily, either by inspection and trial or by solving the set of observation equations involved. In a few cases, the situation has been more complicated and a midway choice has been made, guided by the principle of least squares, that the sum $\sum_j w_j \cdot \Delta_j^2$ over the reactions involved should be the smallest for the adopted values. The final adjusted Q values are listed in column 4 of Table IV. For the 40 Q values in group (A), the amounts of adjustment are all within the respective probable error of the experimental values, except item 19 of Table IV, where the experimental value of 6.797 ± 0.008 has been adjusted to 6.808 ± 0.006, the adjustment of 11 kev exceeds the experimental probable error of 8 kev. A summary of the adjustments made is shown in Table IVa.

After adjustment the 40 Q values are numerically consistent to one kev. This one kev is due to the rounding off of the last figures. Once the set of numerically consistent set of Q values has been determined the calculation of the masses is straightforward, with some care in handling the errors. Any long chain leading from O^{16} to H^1 gives the hydrogen mass. The four fundamental mass differences in Table V give immediately the n, H^1, H^2, H^3 and He^4 masses, and the remaining

masses from the adjusted Q values. The values of the same mass obtained by taking different paths differ by 2 kev in the extreme case, less than one tenth of the probable error of the mass. The mass excess M - A in terms of Mev has been derived directly from the adjusted Q values, using the path which gives the smallest resultant probable error. It has been converted to mass units by the factor 931.15 ± 0.01 Mev/amu(34). The masses are thereby obtained by adding the respective mass or mass number, so that the conversion factor need not enter into the calculation unnecessarily.

Masses of the Remaining Nuclei.

The cycle containing F^{19}, O^{16} and O^{17} has been adjusted to give a zero sum and thereby yields the masses F^{19} and O^{17}. F^{20} and the masses in group (C) have been calculated from experimental Q values and the adjusted values of the masses obtained above. For example, F^{20} was calculated from the experimental value of $F^{19}(d,p)F^{20}$ with the adjusted masses of F^{19}, H^1 and H^2.

Table of Atomic Masses of Light Nuclei.

Table VII gives the masses of nuclei thus determined. Masses of the nuclei that can be approached only by reactions whose reaction energies are known with less accuracy have not been included.

The four key masses, H^1, H^2, He^4 and C^{12} from recent mass spectroscopic measurements are included for comparison. The values given in Elementary Nuclear Theory by H. A. Bethe are also listed.

Comparison with Mass Spectroscopic Measurements.

In all modern precision mass spectrographic measurement,

a system of three easily accessible substandards, viz., the nuclei H^1, H^2 and C^{12} are used, relating to the standard $O^{16} = 16$ (35). These are determined with the help of three fundamental doublets:

$$C^{12}H^1{}_4{}^+ - O^{16}{}^+ = \alpha \qquad \text{at mass number 16,}$$
$$H^2{}_3{}^+ - C^{12}{}^{++} = \beta \qquad \text{at mass number 6,}$$
$$H^1{}_2{}^+ - H^2{}^+ = \gamma \qquad \text{at mass number 2.}$$

Hence, one finds for the atomic masses,

$$H^1 = 1 + 1/16\,\alpha + 1/8\,\beta + 3/8\,\gamma$$
$$H^2 = 2 + 1/8\,\alpha + \tfrac{1}{4}\,\beta - \tfrac{1}{4}\,\gamma$$
$$C^{12} = 12 + 3/4\,\alpha - \tfrac{1}{2}\,\beta - 3/2\,\gamma .$$

The extra electrons to make the ions neutral happen to cancel out.

Some measurements of these substandards have been included in Table VI for comparison. No attempt has been made to make a critical survey of all the mass spectroscopic measurements carried out in recent years at different places. The adjusted Q values have been used to compute the equivalent values of the mass doublets from nuclear data.

A glance at Table VI reveals that the agreement between mass spectroscopic data and nuclear data ranges from excellent to bad. The doublets $2H^1 - H^2$ and $2H^2 - He^4$ are satisfactory. The doublet $3H^2 - \frac{1}{2}C^{12}$ gives a large discrepancy. The mass spectroscopic measurements of this doublet were always much lower than the present nuclear result. The measurement on the doublet $C^{12} + 4H^1 - O^{16}$ were sometimes higher, sometimes lower, than the present nuclear result. The masses of the four key masses H^1, H^2, He^4 and C^{12} have been calculated from recent mass spectroscopic measurements and listed in column 5 of Table VII.

No single change in one Q only can be found which would remove the disagreement between mass spectroscopic data and the nuclear results in the doublet values containing C^{12}. Nor can an assumed change in the mass of He remove it. Further measurements seem to be necessary. For the nuclear reactions, cross links (Fig. 12) around $C^{13}(d,\alpha)B^{11}$ and $O^{16}(d,\alpha)N^{14}$ are very desirable, and accurate connections between nuclei below and above O^{16} will extend the accurate mass table further upward.

Table IV. Nuclear Reaction Energies

Used in Evaluating Masses

Reaction	Experimental Q value (mev)	Weighted mean of experimental Q (mev)	Adjusted value of Q (mev)	Ref.
$n(\beta^-)H^1$	0.783 ± .013[a]		0.7824 ± .001	Ro 50p
$H^1(n,\gamma)H^2$	2.230 ± .007			Be 50g
$H^2(\gamma,n)H^1$	-2.226 ± .003	$H^1(n,\gamma)H^2$ =	2.225 ± .002	Mo 50p
$H^2(p,n)2H^1$	-2.225 ± .010	2.227 ± .003		Sm 50b
$H^2(n,\gamma)H^3$	6.251 ± .008		6.257 ± .004	Ki 50p
$H^2(d,n)He^3$	3.265 ± .009[b]		3.268 ± .004	To 49a
$H^2(d,p)H^3$	4.036 ± .012[b]	4.031 ± .005	4.032 ± .004	To 49a
	4.030 ± .006			St 51
$H^3(\beta^-)He^3$	0.0186 ± .0002	0.0185 ± .0002	0.0185 ± .0002	Je 49, Sl 49
	0.0183 ± .0003			Cu 49b
	0.0180 ± .0005			Gr 49
	0.0190 ± .0005			Ha 49b
$H^3(p,n)He^3$	-0.7637 ± .001	$H^3(p,n)He^3$ =		Ta 49c
$He^3(n,p)H^3$	0.766 ± .010	-0.7639 ± .001	-0.7639 ± .001	Fr 50
$He^6(\beta^-)Li^6$	3.215 ± .015		(unadjustable)	Pe 50
$Li^6(p,a)He^3$	4.017 ± .012[b]	4.019 ± .005	4.018 ± .005	To 49b
	4.021 ± .006			St 51
	3.97 ± .03			Bu 50e
$Li^6(d,p)Li^7$	5.019 ± .007		5.020 ± .006	St 51
$Li^7(p,n)Be^7$	-1.6457 ± .002	-1.6453 ± .001[c]		He 49
	-1.6450 ± .002		-1.6453 ± .001	Sh 49d
$LI^7(p,a)a$	17.340 ± .014	17.339 ± .009	17.337 ± .007	St 50p
	17.338 ± .011			Wh 50e
$Li^7(d,p)Li^8$	-0.187 ± .010	-0.188 ± .006	(unadjustable)	Pa 50
	-0.188 ± .007			St 51
$Be^8(a)a$	0.101 ± .010[d]	0.096 ± .004	0.097 ± .004	He 49b
	0.095 ± .005			To 51p

$Be^9(\gamma,n)Be^8$	-1.666 ± .002		-1.666 ± .002	Mo 50p
$Be^9(n,\gamma)Be^{10}$	6.797 ± .008		6.808 ± .006	Ki 50a
$Be^9(p,n)B^9$	-1.852 ± .002		(unadjustable)	Ri 50
$Be^9(p,d)Be^8$	0.558 ± .003 0.562 ± .004	0.560 ± .002	0.560 ± .002	To 49b St 51
$Be^9(p,a)Li^6$	2.121 ± .007[b] 2.142 ± .006	2.133 ± .007	2.132 ± .006	To 49b St 51
$Be^9(d,p)Be^{10}$	4.585 ± .008 4.591 ± .008	4.588 ± .006	4.583 ± .005	St 51 Kl 51
$Be^9(d,t)Be^8$	4.597 ± .013		4.591 ± .004	St 51
$Be^9(d,a)Li^7$	7.150 ± .008 7.151 ± .010 7.191 ± .024	7.153 ± .006	7.152 ± .005	St 51 Wh 50e Kl 51
$Be^{10}(\beta^-)B^{10}$	0.553 ± .015 0.545 ± .010 0.555 ± .005 0.560 ± .005	0.556 ± .003	0.556 ± .003	Fu 49b Be 50 Fe 50 Hu 50b
$B^{10}(n,a)Li^7$	2.793 ± .027 2.788 ± .010	2.789 ± .009	2.795 ± .003	Ha 50p Je 50, El 48
$B^{10}(p,a)Be^7$	1.148 ± .006 1.152 ± .004 1.147 ± .010	1.151 ± .003	1.150 ± .003	Br 50a Va 50 Bu 50
$B^{10}(d,p)B^{11}$	9.235 ± .011		9.235 ± .009	St 51
$B^{11}(p,n)C^{11}$	-2.762 ± .003		(unadjustable)	Ri 50
$B^{11}(p,a)Be^8$	8.567 ± .011 8.574 ± .014	8.570 ± .009	8.575 ± .006	St 51 Li 51
$B^{11}(d,p)B^{12}$	1.136 ± .005		(unadjustable)	St 51
$B^{11}(d,a)Be^9$	8.018 ± .007		8.015 ± .006	Va 51p
$C^{12}(n,\gamma)C^{13}$	4.947 ± .010		4.947 ± .005	Ki 50a
$C^{12}(d,n)N^{13}$	-0.281 ± .003		-0.281 ± .003	Bo 49c
$C^{12}(d,p)C^{13}$	2.716 ± .005 2.732 ± .006	2.723 ± .005	2.722 ± .004	St 51 KI 51

$C^{13}(p,n)N^{13}$	-3.003 ± .003		-3.003 ± .002	Ri 50
$C^{13}(d,p)C^{14}$	5.91 ± .03	5.941 ± .004	5.942 ± .004	Cu 50
	5.948 ± .008			St 51
	5.940 ± .004			Li 51
$C^{13}(d,t)C^{12}$	1.310 ± .006	1.310 ± .003	1.310 ± .003	St 51
	1.310 ± .003			Li 51
$C^{13}(d,a)B^{11}$	5.160 ± .010	5.163 ± .005	(unadjustable)	St 50p
	5.164 ± .006			Li 51
$C^{14}(\beta^-)N^{14}$	0.154 ± .003	0.155 ± .001	0.155 ± .001	Le 47a
	0.152 ± .005			Le 48a
	0.1563 ± .001			Co 48c
	0.155 ± .002			Be 48b
	0.1575 ± .005			An 49b
	0.155 ± .001			Fe 49
	0.155 ± .001			Wa 50b
$C^{14}(p,n)N^{14}$	-0.620 ± .009	$C^{14}(p,n)N^{14}$ =		Sh 49a
$N^{14}(n,p)C^{14}$	0.630 ± .006	-0.628 ± .004	-0.627 ± .001	Fr 50
	0.630 ± .010			St 48a
$N^{13}(\beta^+)C^{13}$	2.220 ± .006	2.222 ± .004	2.221 ± .002	Ly 39
	2.224 ± .005			Ho 50
$N^{14}(n,\gamma)N^{15}$	10.823 ± .012		10.834 ± .007	Ki 50a
$N^{14}(d,p)N^{15}$	8.615 ± .009		8.609 ± .007	St 51
$N^{15}(p,a)C^{12}$	4.960 ± .007	4.961 ± .005	4.961 ± .005	St 51
	4.961 ± .006			Li 51
$N^{15}(d,a)C^{13}$	7.681 ± .009		7.683 ± .006	St 51
$O^{15}(\beta^+)N^{15}$	2.705 ± .005		(unadjustable)	Pe 49p
$O^{16}(d,n)F^{17}$	-1.614 ± .010[e]		(unadjustable)	He 48a
$O^{16}(d,p)O^{17}$	1.917 ± .007	1.917 ± .005	1.919 ± .005	St 51
	1.918 ± .008			Kl 51
$O^{16}(d,a)N^{14}$	3.112 ± .006	3.116 ± .004	(unadjustable)	St 50p
	3.119 ± .005			Wh 51
$O^{18}(p,n)F^{18}$	-2.453 ± .002		-2.453 ± .002	Ri 50p
$F^{18}(\beta^+)O^{18}$	1.657 ± .015		1.671 ± .002	Bl 49a
$F^{19}(p,a)O^{16}$	8.113 ± .030	8.118 ± .009	8.124 ± .007	Ch 50
	8.118 ± .009			St 51

$F^{19}(d,p)F^{20}$	4.373 ± .007	(unadjustable)	St 51
$F^{19}(d,a)O^{17}$	10.050 ± .010	10.043 ± .007	St 51

---

[a] The recoil energy of the proton included.

[b] Probable error recalculated according to the systematic procedure outlined in Brown et al, Phys. Rev. (in press).

[c] -1.6457 ± .002 mev has been used as a standard in many of the experimental Q values in this table. This corresponds to a threshold energy of 1.882 ± .002 mev.

[d] Recalculated with recent values of ThC" gamma ray energy and $Be^9(\gamma,n)Be^8$ threshold.

[e] Corrected to $Li^7(p,n)Be^7$ threshold = 1.882 mev.

References

The designation in the last column of the table refers to the reference list in Hornyak, Lauritsen, Morrison, and Fowler, Rev. Mod. Phys. 22, 364, (1950).

In addition:

Ha 50p Hanna, Phys. Rev. 80, 530 (1950)
Ki 50p Kinsey and Bartholomew, Phys. Rev. 80, 918 (1950)
Kl 51 Klema and Phillips, private communication.
Li 51 Li and Whaling, Phys. Rev. (in press)
Mo 50p Mobley and Laubenstein, Phys. Rev. 80, 309 (1950)
Pe 49p Perez-Mendez and Brown, Phys. Rev. 76, 689 (1949)
Ri 50p Richards and Smith, Phys. Rev. 80, 524 (1950)
Ro 50p Robeson, Phys. Rev. 81, 297 (1951)
St 50p Strait, Van Patter, Sperduto, and Buechner, Phys. Rev. 81, 315 (1951)
St 51 Strait, Van Patter, Buechner, and Sperduto, Phys. Rev. (in press).
To 51p Tollestrup (private communication)
Va 51p Van Patter, Sperduto, Huang, Strait, and Buechner Phys. Rev. 81, 233 (1951)
Wh 51 Whaling and Li (private communication)

Table IV a. Summary of the Adjustments of the Interlinked Q-values below O^{16}

Amount of adjustment	Number of cases
0 (kev)	13
1	12
2	3
3	2
4	0
5	3
6	3
7	0
8	0
9	0
10	0
11	2
unadjustable	2
Total	40

Sign of adjustment	Number of cases
0	13
+	11
-	14
unadjustable	2
Total	40

Ratio of the adjustment to the probable error of the experimental Q	Number of cases
0 or up to 1/5	20
between 1/5 and $\frac{1}{2}$	10
between $\frac{1}{2}$ and 1	7
11/8	1
unadjustable	2
Total	40

Table IV b. Q-values, each with an error greater than 2 kev and adjustable by more than one cycle.

Reaction	Experimental Q	Q adjusted from one cycle	From which cycle	Final adjusted value
$H^2(d,n)He^3$	3.265 ± .009	3.268 ± .004 3.266 ± .008	$n - H^1$ $2H^2 - He^4$	3.268 ± .004
$Li^6(d,p)Li^7$	5.019 ± .007	5.019 ± .006 5.020 ± .006	zero $2H^2 - He^4$	5.020 ± .006
$Li^7(p,\alpha)\alpha$	17.339 ± .009	17.337 ± .007 17.340 ± .008	$2H^2 - He^4$ $2H^2 - He^4$	17.337 ± .007
$Be^9(d,p)Be^8$	4.588 ± .006	4.589 ± .005 4.582 ± .006	$n - H^1$ $n + H^1 - H^2$	4.583 ± .005
$Be^9(d,\alpha)Li^7$	7.153 ± .006	7.153 ± .005 7.152 ± .005 7.152 ± .006 7.152 ± .006	zero $n - H^1$ $2H^2 - He^4$ $2H^2 - He^4$	7.152 ± .005
$B^{10}(n,\alpha)Li^7$	2.789 ± .009	2.795 ± .003 2.790 ± .006 2.792 ± .008	zero $n - H^1$ $2H^2 - He^4$	2.795 ± .003
$B^{11}(d,\alpha)Be^9$	8.018 ± .007	8.015 ± .006 8.016 ± .006	zero $2H^2 - He^4$	8.015 ± .006
$C^{12}(d,p)C^{13}$	2.723 ± .005	2.722 ± .004 2.723 ± .004 2.723 ± .005 2.722 ± .004	zero $n - H^1$ $n + H^1 - H^2$ $2H^2 - H^1 - H^3$	2.722 ± .004
$N^{14}(n,p)C^{14}$	0.628 ± .004	0.627 ± .001 0.627 ± .004	$n - H^1$ $2H^2 - He^4$	0.627 ± .001
$N^{13}(\beta^+)C^{13}$	2.222 ± .004	2.221 ± .002 2.222 ± .003	$n - H^1$ $n - H^1$	2.221 ± .002
$N^{14}(n,\gamma)N^{15}$	10.823 ± .012	10.834 ± .007 10.831 ± .009	$n + H^1 - H^2$ $2H^2 - He^4$	10.834 ± .007
$N^{15}(d,\alpha)C^{13}$	7.681 ± .009	7.683 ± .006 7.686 ± .008	zero $2H^2 - He^4$	7.683 ± .006

Table V. Nuclear Cycles and Fundamental Mass Differences

Cycle	Mass difference from experimental Q (Mev)
Group 1. Nuclear cycles giving a sum of zero.	
$Be^9(p,\alpha)Li^6$, $Li^6(d,p)Li^7$, $Be^9(d,\alpha)Li^7$	0.001 ± 0.012
$B^{11}(p,\alpha)Be^8$, $Be^9(p,d)Be^8$, $B^{11}(d,\alpha)Be^8$	0.008 ± 0.012
$N^{15}(p,\alpha)C^{12}$, $C^{12}(d,p)C^{13}$, $N^{12}(d,\alpha)C^{13}$	0.003 ± 0.011
$B^{10}(n,\alpha)Li^7$, $Li^7(p,n)Be^7$, $B^{10}(p,\alpha)Be^7$	0.007 ± 0.010
$F^{19}(p,\alpha)O^{16}$, $O^{16}(d,p)O^{17}$, $F^{19}(d,\alpha)O^{17}$	0.015 ± 0.014
Group 2. $n - H^1$.	
$n(\beta^-)H^1$	0.783 ± 0.013
$H^3(p,n)He^3$, $H^3(\beta^-)He^3$	0.7824 ± 0.001
$C^{13}(p,n)N^{13}$, $N^{13}(\beta^+)C^{13}$	0.781 ± 0.005
$C^{14}(p,n)N^{14}$, $C^{14}(\beta^-)N^{14}$	0.783 ± 0.004
$O^{18}(p,n)F^{18}$, $F^{18}(\beta^+)O^{18}$	0.796 ± 0.015
$H^2(d,p)H^3$, $H^2(d,n)He^3$, $H^3(\beta^-)He^3$	0.7845 ± 0.010
$C^{12}(d,p)C^{13}$, $C^{12}(d,n)N^{13}$, $N^{13}(\beta^+)C^{13}$	0.782 ± 0.007
$B^{10}(n,\alpha)Li^7$, $Be^9(d,\alpha)Li^7$, $Be^9(d,p)Be^{10}$, $Be^{10}(\beta^-)B^{10}$	0.780 ± 0.013
Weighted mean of $n - H^1$ =	0.7824 ± 0.001
(p_e = 0.23 kev, p_i = 0.93 kev, p_e/p_i = 0.25)	
Group 3. $n + H^1 - H^2$.	
$H^1(n,\gamma)H^2$	2.227 ± 0.003
$H^2(d,p)H^3$, $H^2(n,\gamma)H^3$	2.220 ± 0.009

Be^9 (p,d)Be^8, $Be^9(\gamma,n)Be^8$	2.226 ± 0.003
$Be^9(d,p)Be^{10}$, $Be^9(n,\gamma)Be^{10}$	2.209 ± 0.010
$C^{12}(d,p)C^{13}$, $C^{12}(n,\gamma)C^{13}$	2.224 ± 0.011
$N^{14}(d,p)N^{15}$, $N^{14}(n,\gamma)N^{15}$	2.208 ± 0.015
Weighted mean of $n + H^1 - H^2$ =	2.225 ± 0.002

(p_e = 1.3 kev, p_i = 1.9 kev, p_e/p_i = 0.68)

Group 4. $2H^2 - H^1 - H^3$.

$H^2(d,p)H^3$	4.031 ± 0.005
$Be^9(p,d)Be^8$, B $e^9(d,t)Be^8$	4.037 ± 0.013
$C^{12}(d,p)C^{13}$, $C^{13}(d,t)C^{12}$	4.033 ± 0.006
Weighted mean of $2H^2 - H^1 - H^3$ =	4.032 ± 0.004

Group 5. $2H^2 - He^4$.

$Li^7(p,\alpha)He^4$, $Be^8(\alpha)\alpha$, $Be^9(p,d)Be^8$, $Be^9(d,\alpha)Li^7$	23.836 ± 0.012
$N^{15}(d,\alpha)C^{13}$, $C^{13}(d,p)C^{14}$, $C^{14}(p,n)N^{14}$, $N^{14}(n,\gamma)N^{15}$	23.817 ± 0.016
B^{10} $(n,\alpha)Li^7$, $Be^9(d,\alpha)Li^7$, $B^{11}(d,\alpha)Be^9$, $B^{10}(d,p)B^{11}$ with $n + H^1 - H^{2*}$	23.842 ± 0.017
$Li^7(p,\alpha)He^4$, $Li^6(d,p)Li^7$, $Li^6(p,\alpha)He^3$, $H^2(d,n)He^3$ with $n + H^1 - H^{2*}$	23.829 ± 0.015
Weighted mean of $2H^2 - He^4$ =	23.832 ± 0.007

* $n + H^1 - H^2$ = 2.225 ± 0.002 Mev from the weighted mean in this table.

Table VI. Fundamental Mass Spectroscopy Doublets

	Computed from nuclear data (mMU)*	From mass spectroscopy (mMU)		
		Most probable values listed by Bainbridge (1948)[a]	Roberts and Nier; Nier (1950)[b,c]	Ewald (1950)[d]
$2H^1 - H^2$	1.550 ± .0024	1.5380 ± .0021	1.549±.006 †	
$2H^2 - He^4$	25.594 ± .008	(25.587 ± .032)	25.612 ± .008†	25.604±.009 †
$3H^2 - 1/2\ C^{12}$	42.298 ± .016	42.228 ± .019†		
$C^{12} + 4H^1 - O^{16}$	36.367 ± .019	36.369 ± .021	36.45 ± .022†	
$C^{12} + 2H^1 - N^{14}$	12.570 ± .012	12.566 ± .012	12.61	

[a] K. T. Bainbirdge, NRC Nuclear Science Series, No. 1 (1948).

[b] T. R. Roberts and A. O. Nier, Phys. Rev. 77, 746 (1950).

[c] Quoted in Bainbirdge, Phys. Rev. 81, 147 (1951).

[d] H. Ewald, Zeit, F. Naturforschung 5, 1 (1950).

* 1 mMU = 0.93115 Mev, Dumond and Cohen "Report to NRC Committee on Constants and Conversion Factors of Physics" (1950).

† These values were used in the calculation of the atomic masses from mass spectroscopic data (see Table of Atomic Masses).

Table VII. Table of Atomic Masses

	A mass number		M-A, mass excess (Mev)	M, atomic mass from nuclear date (AMU)* PE x10^6	Atomic Mass from mass spectroscopy †	Bethe PE omitted
n	1	8.3631	.0029	1.008 981 (±3)		1.008 93
H	1	7.5807	.0027	1.008 141 (±3)	1.008 138 (±4)	1.008 123
H	2	13.719	.006	2.014 733 (±6)	2.014 726 (±6)	2.014 708
H	3	15.825	.010	3.016 995 (±11)		3.017 02
He	3	15.806	.010	3.016 975 (±11)		3.017 00
He	4	3.6056	.014	4.003 872 (±15)	4.003 844 (±13)	4.003 90
He	6	19.064	.025	6.020 474 (±27)		6.020 90
Li	6	15.849	.021	6.017 021 (±22)		6.016 97
Li	7	16.967	.024	7.018 222 (±26)		7.018 22
Li	8	23.294	.028	8.025 016 (±30)		8.025 02
Be	7	17.830	.024	7.019 149 (±26)		7.019 16
Be	8	7.308	.027	8.007 849 (±29)		8.007 85
Be	9	14.005	.028	9,015 041 (±30)		9.015 03
Be	10	15.560	.026	10.016 711 (±28)		10.016 77
B	9	15.075	.029	9.016 189 (±31)		9.016 20
B	10	15.004	.026	10.016 114 (±28)		10.016 18
B	11	11.907	.022	11.012 788 (±23)		11.012 84
B	12	16.909	.020	12.018 160 (±22)		12.019 0
C	11	13.887	.022	11.014 914 (±24)		11.014 95
C	12	3.540	.015	12.003 802 (±17)	12.003 900 (±21)	12.003 82
C	13	6.956	.013	13.007 470 (±14)		13.007 51
C	14	7.152	.010	14.007 681 (±11)		14.007 67
N	13	9.177	.013	13.009 856 (±14)		13.009 88
N	14	6.997	.010	14.007 515 (±11)		14.007 51
N	15	4.526	.011	15.004 861 (±12)		15.004 89
O	15	7.231	.012	15.007 766 (±13)		15.007 8
O	16			16.000 000 (standard)		16.000 000
O	17	4.219	.006	17.004 531 (±7)		17.004 50
F	17	6.970	.011	17.007 485 (±11)		17.007 5
F	19	4.149	.014	19.004 456 (±15)		19.004 50
F	20	5.914	.017	20.006 351 (±19)		

* 1 Mev = 1.07394 mMU

† See Table VI.

REFERENCES

1. Snyder, Rubin, Fowler and Lauritsen, Rev. Sci. Inst. 21, 852 (1950).
2. Siegbahn and Svartholm, Arkiv. f. Math. Astron. Fysik 33A, No. 21 (1946); Svartholm, ibid 33A, No. 24 (1946).
3. Shull and Dennison, Phys. Rev. 71, 681 (1947).
4. Shull and Dennison, Phys. Rev. 72, 256 (1947).
5. Rosenblum, Phys. Rev. 72, 731 (1947).
6. Shull, Phys. Rev. 74, 917 (1948).
7. Kurie, Osaba and Slack, Rev. Sci. Inst. 19, 771 (1948).
8. Judd, Rev. Sci. Inst. 21, 213 (1950).
9. Snyder, Thesis, California Institute of Technology (1948).
10. Svartholm, Arkiv. f. Fysik 2, No. 14, 115 (1950); ibid 2, No. 20, 195 (1950).
11. Lauritsen and Lauritsen, Rev. Sci. Inst. 19, 916 (1948).
12. Holloway and Livingston, Phys. Rev. 54, 18 (1938).
13. Rutherford, Chadwick and Ellis, Radiations from Radioactive Substances, McMillan Company (1930), p. 155.
14. Briggs, Proc. Roy. Soc. (London) A157, 183 (1936).
15. Lauritsen, Lauritsen and Fowler, Phys. Rev. 59, 241 (1940).
16. Fowler, Lauritsen and Lauritsen, Rev. Sci. Inst. 18, 818 (1947).
17. Herb, Snowdon and Sala, Phys. Rev. 75, 246 (1949).
18. Tollestrup, Thesis, California Institute of Technology (1950).
19. Brown, et al., Phys. Rev. (in publication).
20. Smith, Phys. Rev. 56, 548 (1939).
21. Bateson, Phys. Rev. 80, 982 (1950).
22. Buechner and Van Patter, Phys. Rev. 79, 240 (1950).
23. Cockcroft and Lewis, Proc. Roy. Soc. 154, 246 (1936).

24. Livingston and Bethe, Rev. Mod. Phys. 9, 245 (1937).

25. Pollard, Davidson and Schultz, Phys. Rev. 57, 1117 (1939).

26. Schardt, Fowler and Lauritsen, Phys. Rev. 80, 136 (1950); Schardt, Thesis, California Institute of Technology (1950).

27. Freeman, Proc. Roy. Soc. (London) 63A, 668 (1950).

28. Tollestrup, Fowler and Lauritsen, Phys. Rev. 78, 372 (1950).

29. Hanson and Benedict, Phys. Rev. 65, 33 (1944).

30. Birge, Phys. Rev. 40, 207 (1932).

31. Townsend, Proc. Roy. Soc. 177, 357 (1940-41).

32. Siegbahn and Bohr, Arkiv. f. Ast. Math. Fysik 30B, No. 3 (1944).

33. Richards and Smith, Phys. Rev. 77, 752 (1950).

34. DuMond and Cohen, Report to the NRC Committer on Constants and Conversion Factors of Physics (1950).

35. Mattauch and Flügge, Nuclear Physics Tables, Interscience Publishers (1946).

Fig. 1.

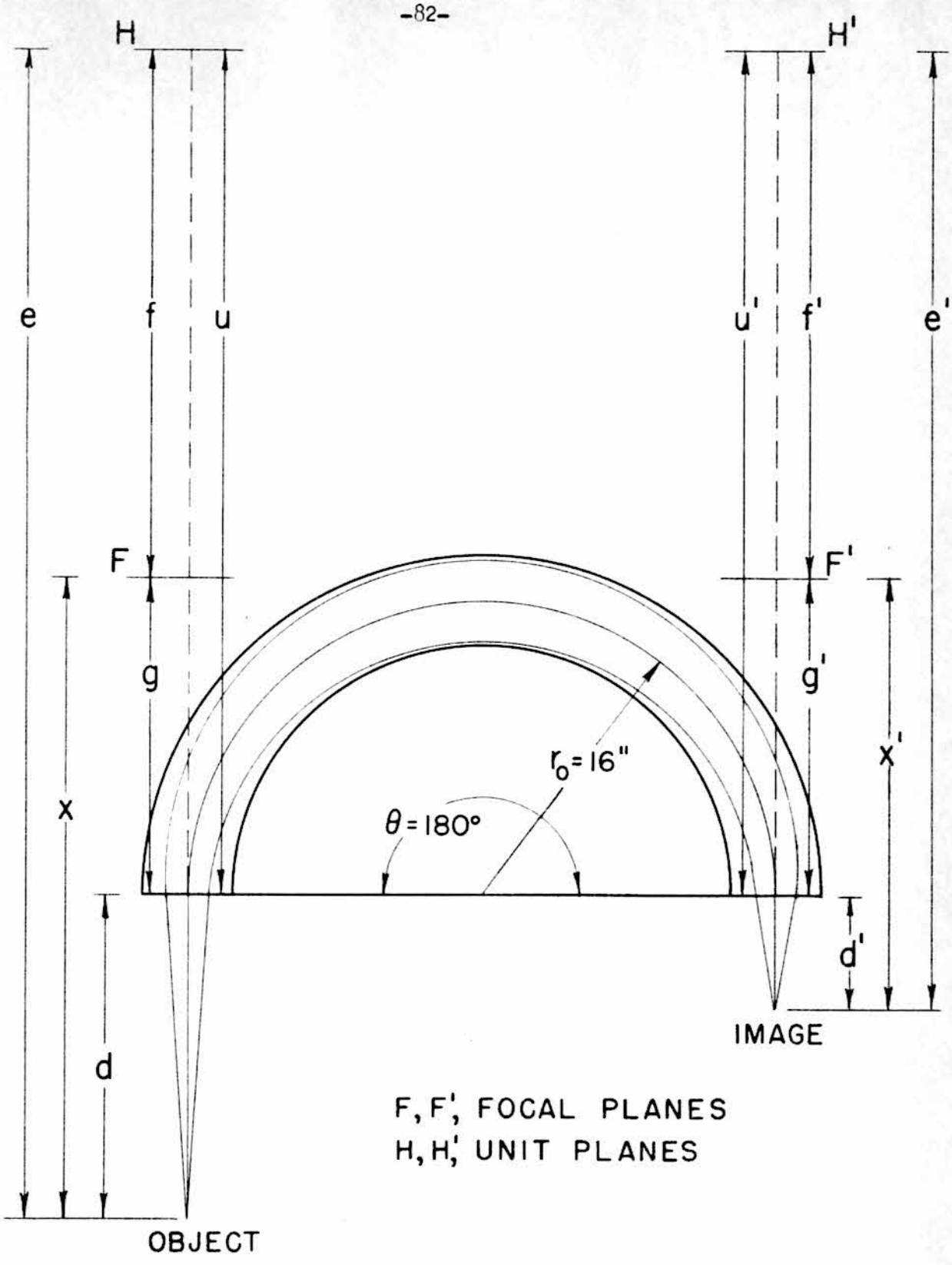

CONSTANTS OF THE 16" SPECTOGRAPH AS A MAGNETIC LENS

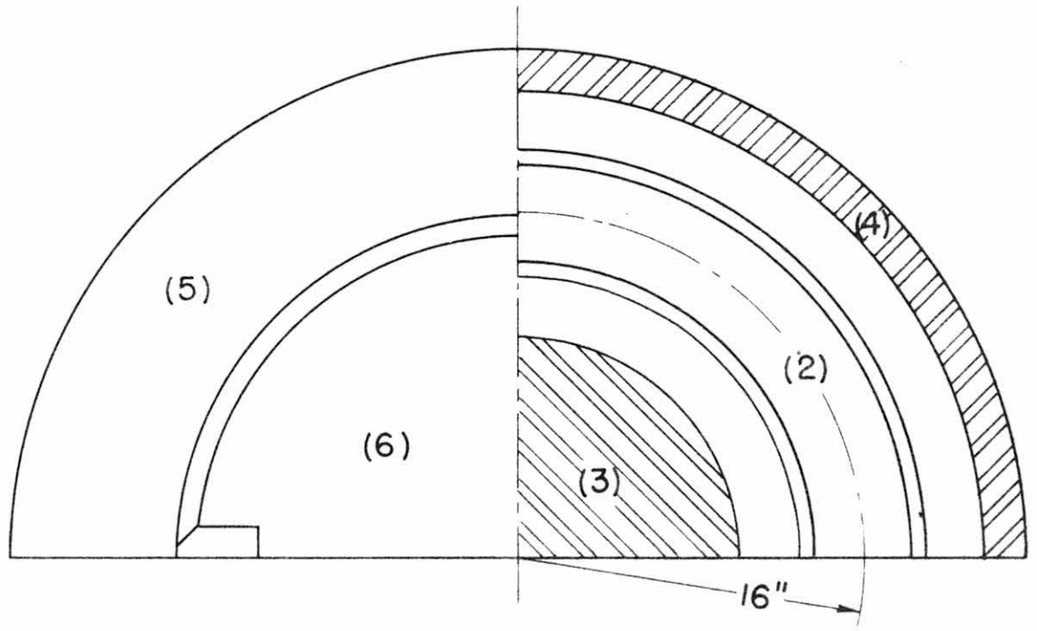

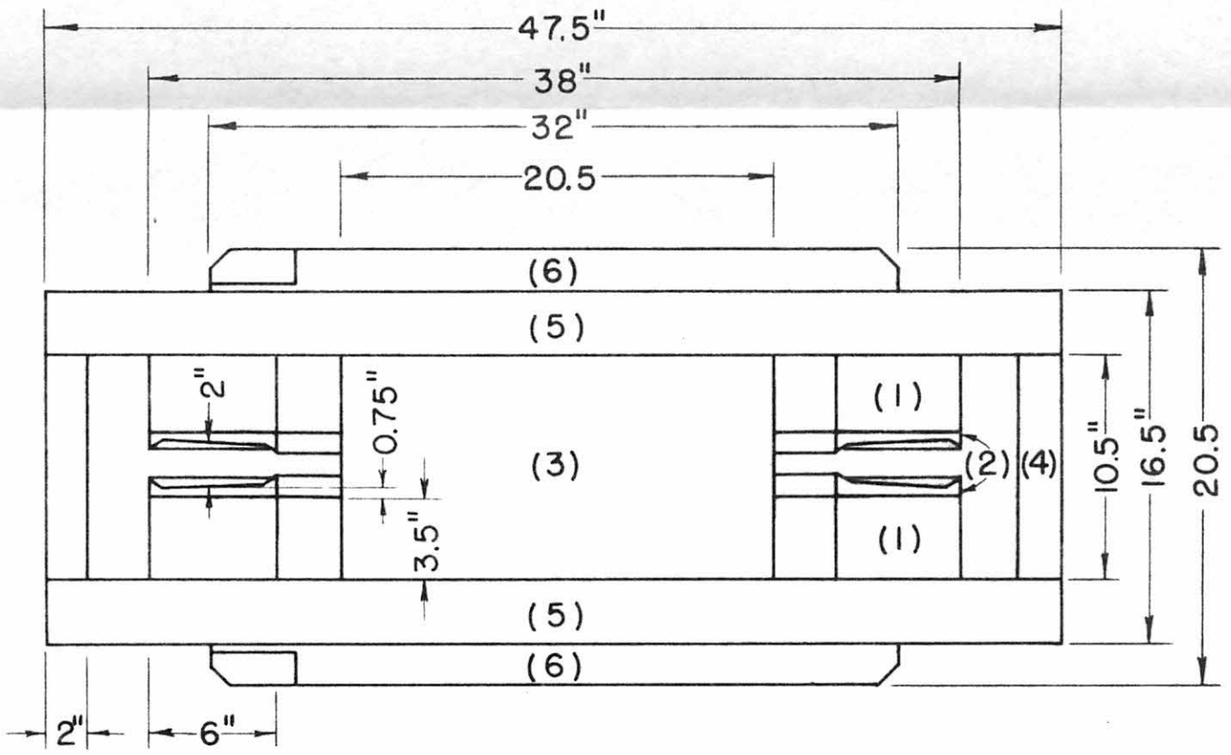

(1) POLE PIECE

(2) POLE FACE

(3) INNER RETURN

(4) OUTER RETURN

(5) INNER YOKE

(6) OUTER YOKE

THE MAGNET BODY

Fig. 2.

Fig. 3.

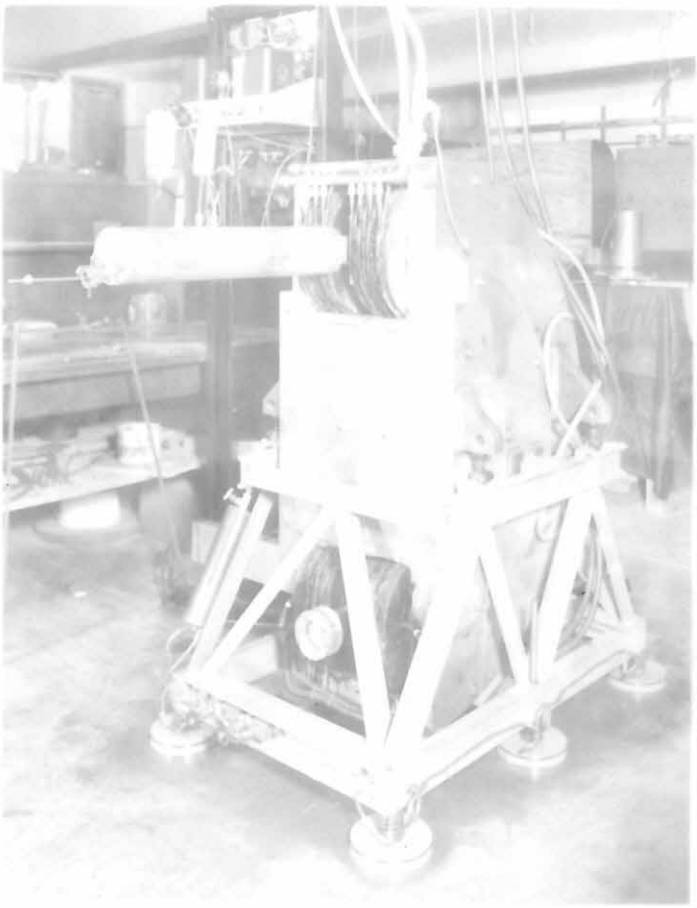

Fig. 4.

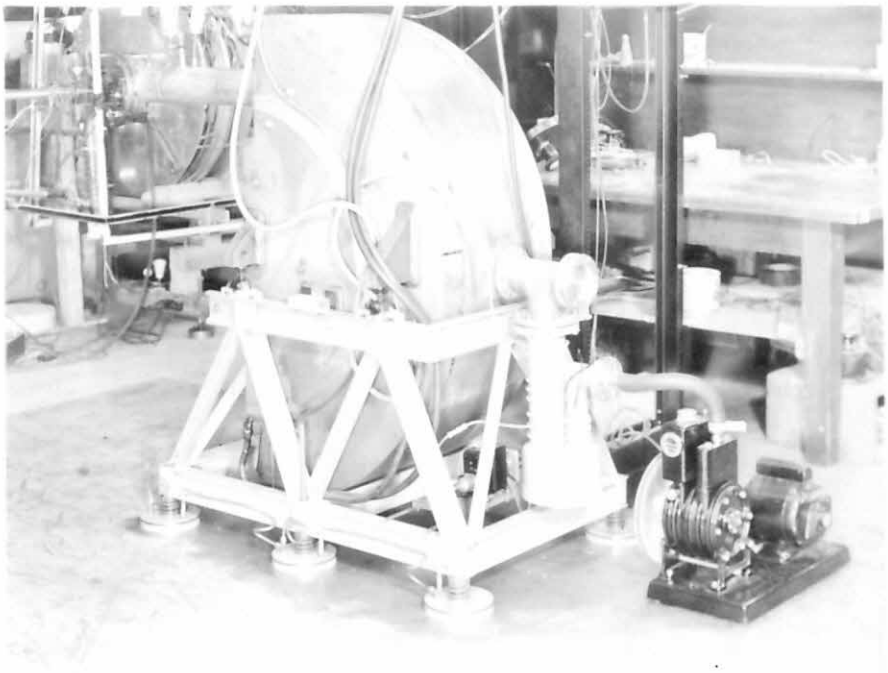

Fig. 5.

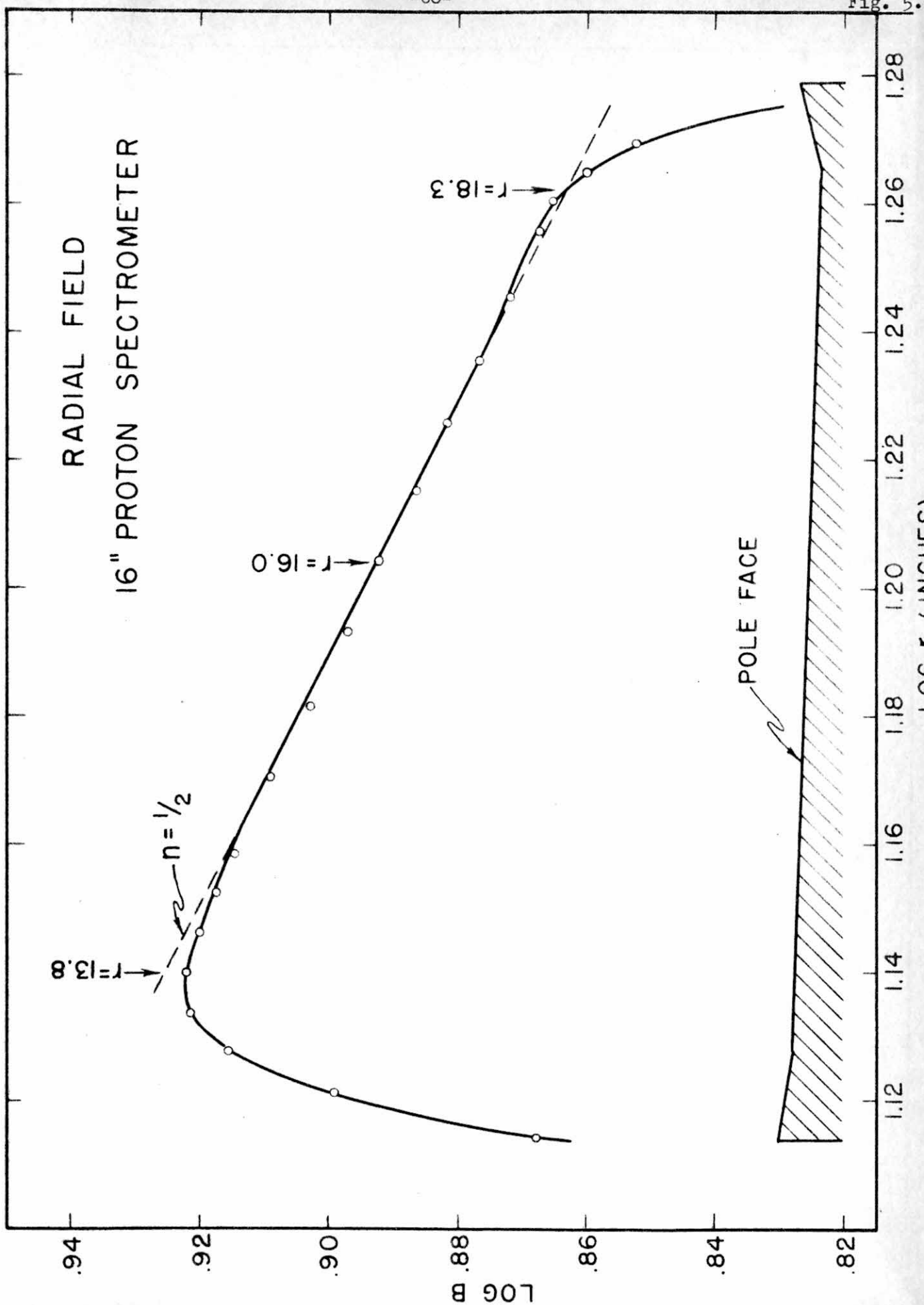
RADIAL FIELD
16" PROTON SPECTROMETER
r = 18.3
r = 16.0
n = 1/2
r = 13.8
POLE FACE
LOG B
LOG r (INCHES)
.94
.92
.90
.88
.86
.84
.82
1.12
1.14
1.16
1.18
1.20
1.22
1.24
1.26
1.28

Fig. 6.

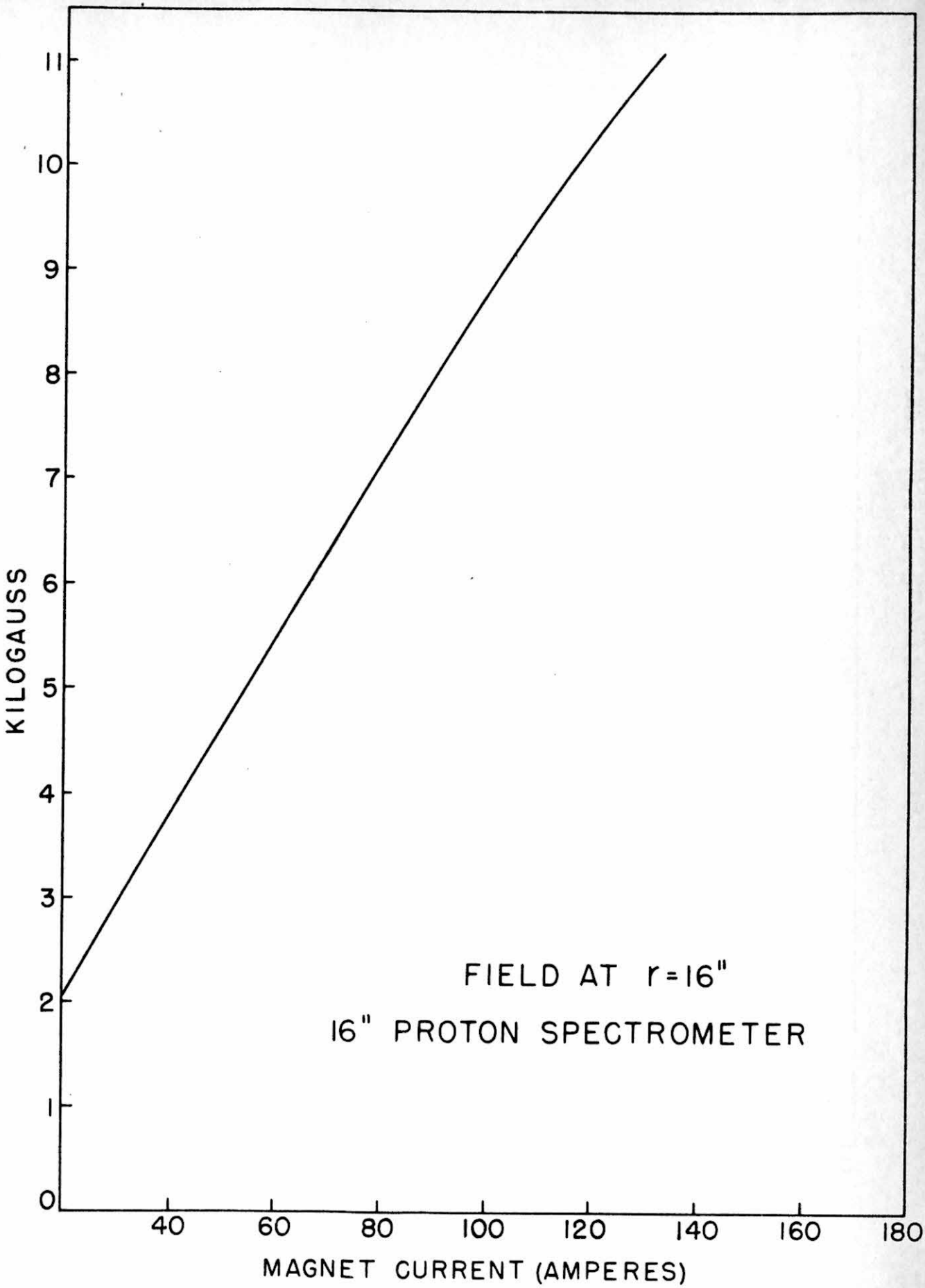
KILOGAUSS
0
1
2
3
4
5
6
7
8
9
10
11
40
60
80
100
120
140
160
180
MAGNET CURRENT (AMPERES)
FIELD AT r=16"
16" PROTON SPECTROMETER

Fig. 7.

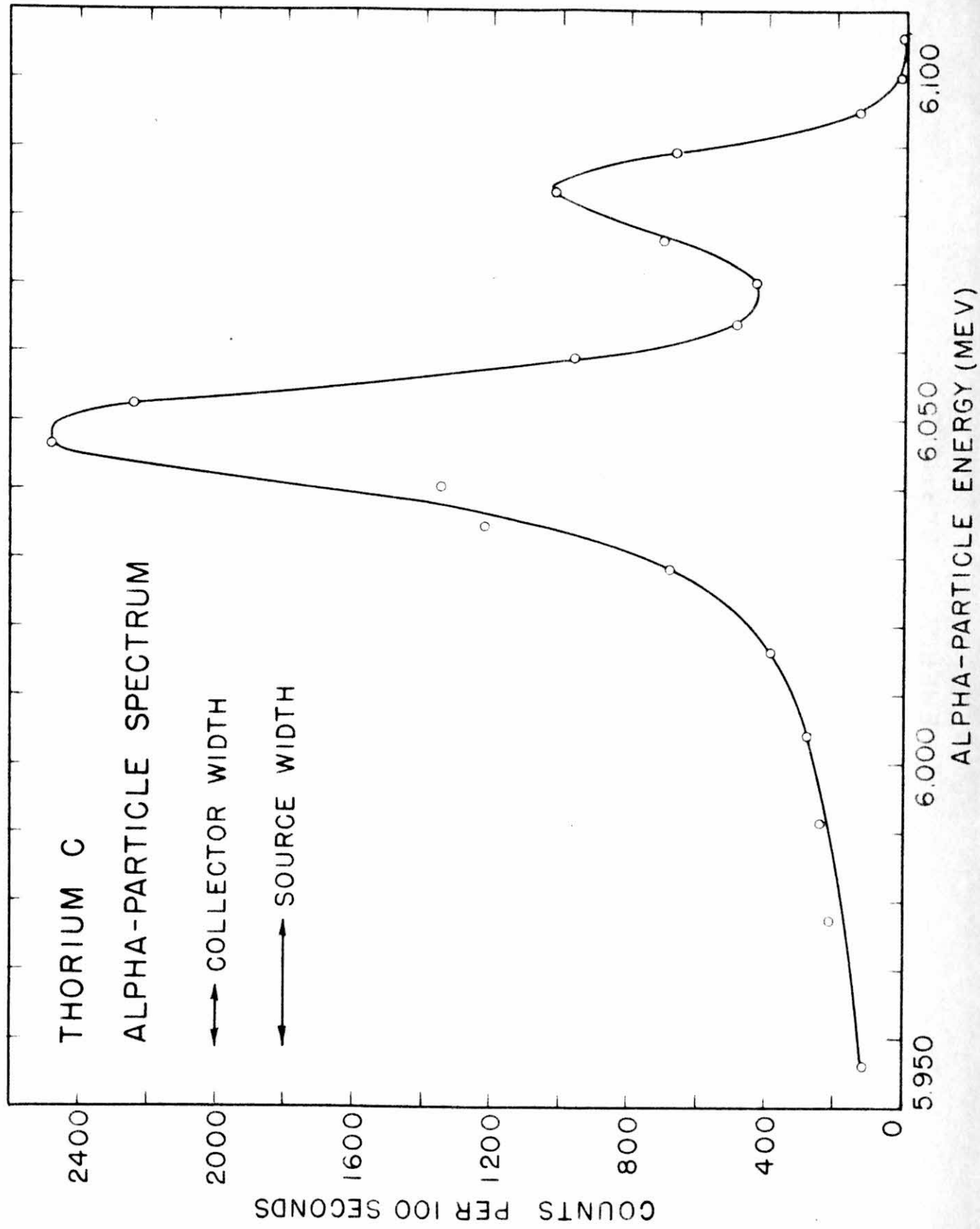
THORIUM C
ALPHA-PARTICLE SPECTRUM
COLLECTOR WIDTH
SOURCE WIDTH
COUNTS PER 100 SECONDS
0
400
800
1200
1600
2000
2400
5.950
6.000
6.050
6.100
ALPHA-PARTICLE ENERGY (MEV)

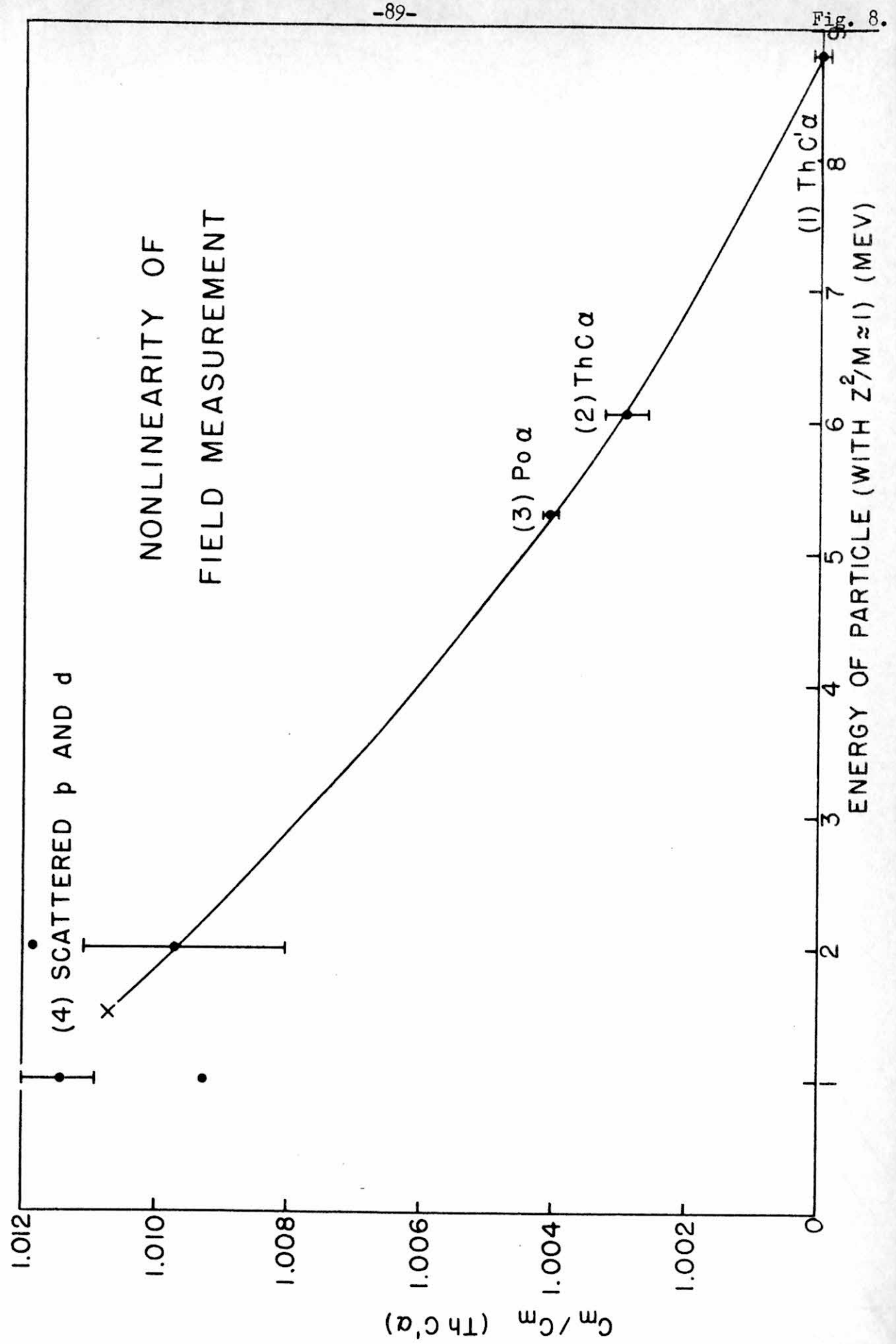
NONLINEARITY OF
FIELD MEASUREMENT
(4) SCATTERED p AND d
(3) Po α
(2) ThC α
(1) ThC'α
1.012
1.010
1.008
1.006
1.004
1.002
0
1
2
3
4
5
6
7
8
9
ENERGY OF PARTICLE (WITH Z²/M≈1) (MEV)
Cm / Cm (ThC'α)

Fig. 8.

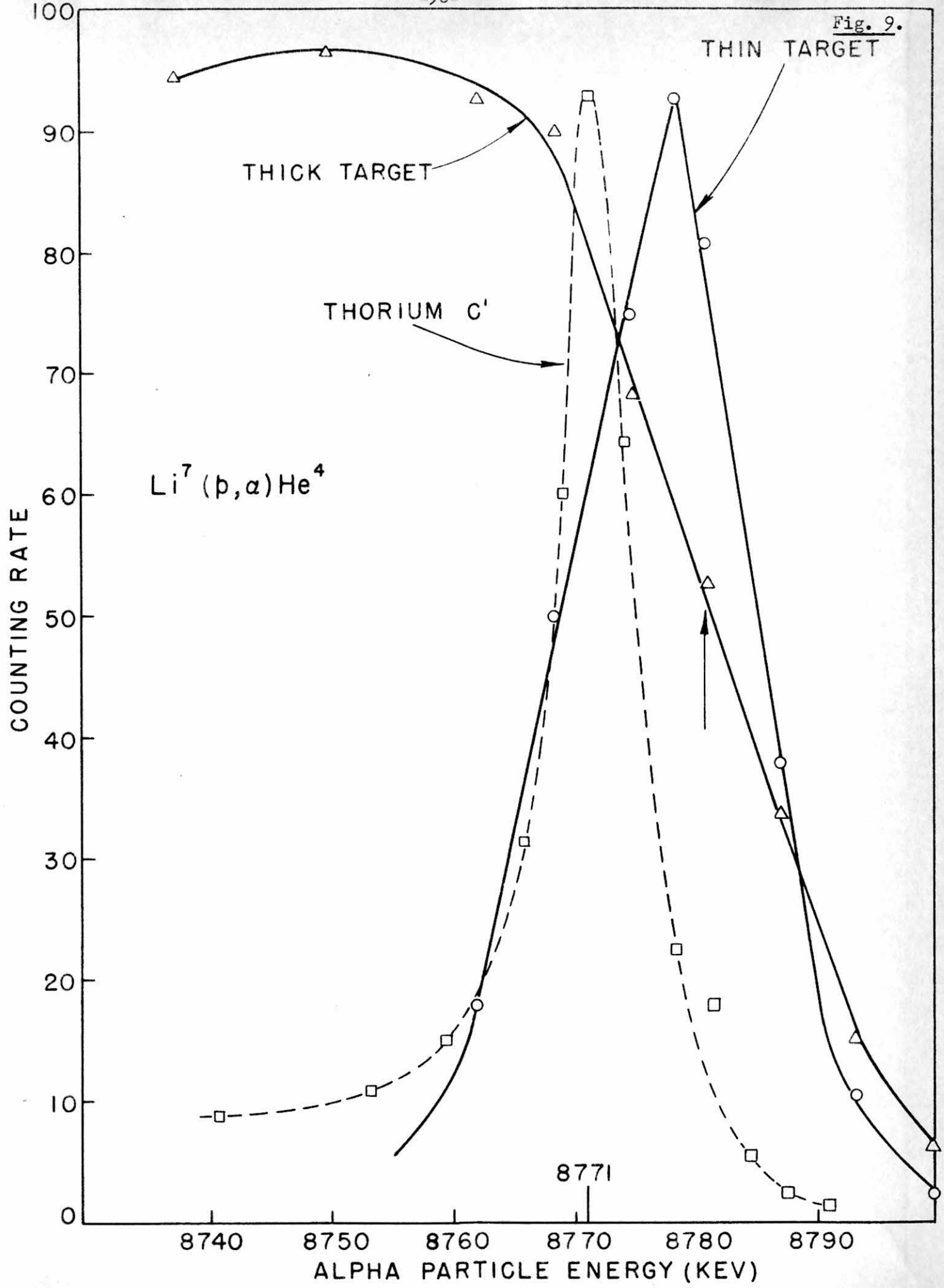
Fig. 9.
THIN TARGET
THICK TARGET
THORIUM C'
$Li^7(p,\alpha)He^4$
COUNTING RATE
100
90
80
70
60
50
40
30
20
10
0
8740
8750
8760
8770
8780
8790
8771
ALPHA PARTICLE ENERGY (KEV)

Fig. 10.

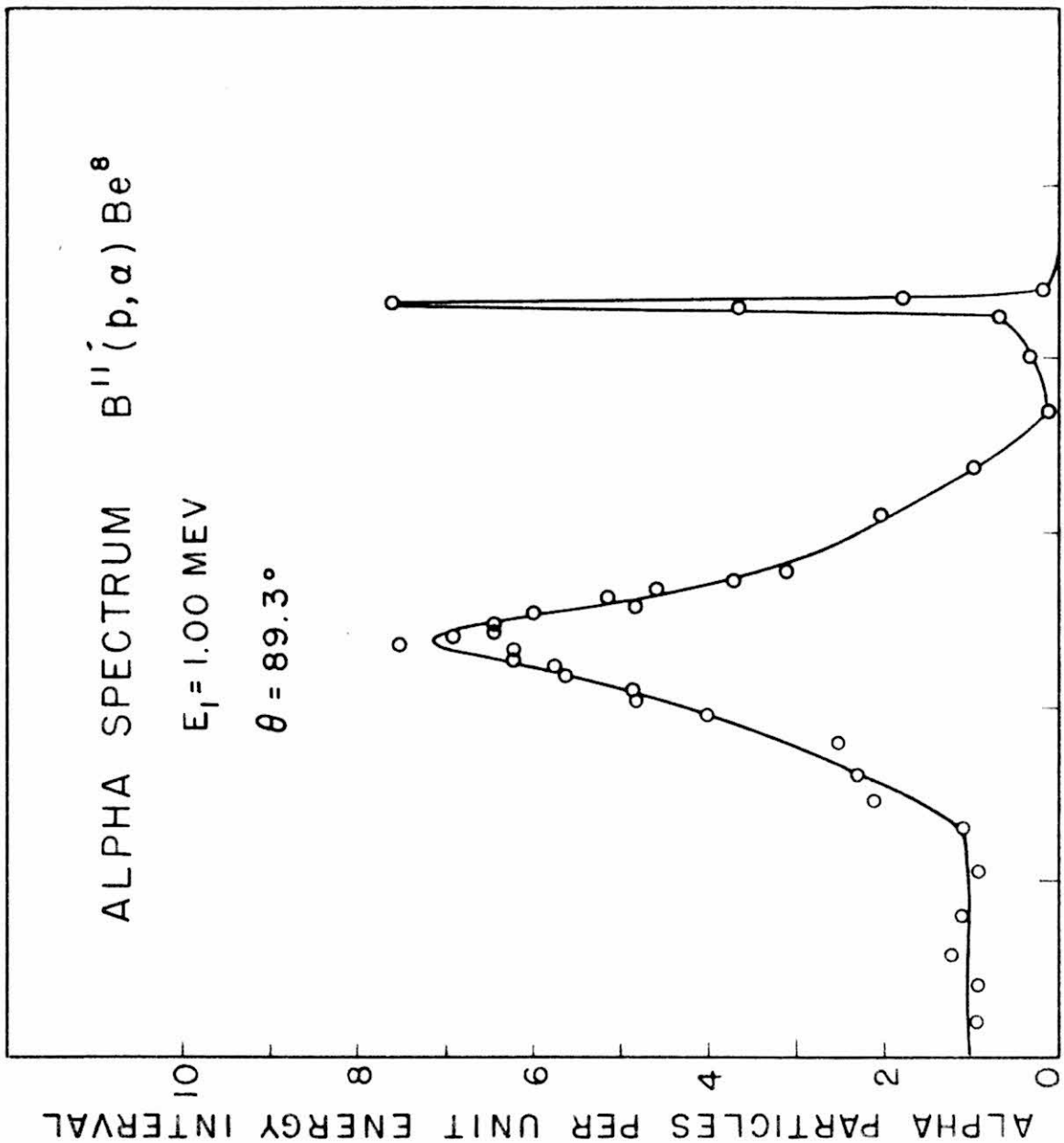
ALPHA SPECTRUM B''(p,α) Be⁸
E_I = 1.00 MEV
θ = 89.3°
ALPHA PARTICLES PER UNIT ENERGY INTERVAL
E_α MEV
0
2
4
6
8
10
2
3
4
5
6
7
8

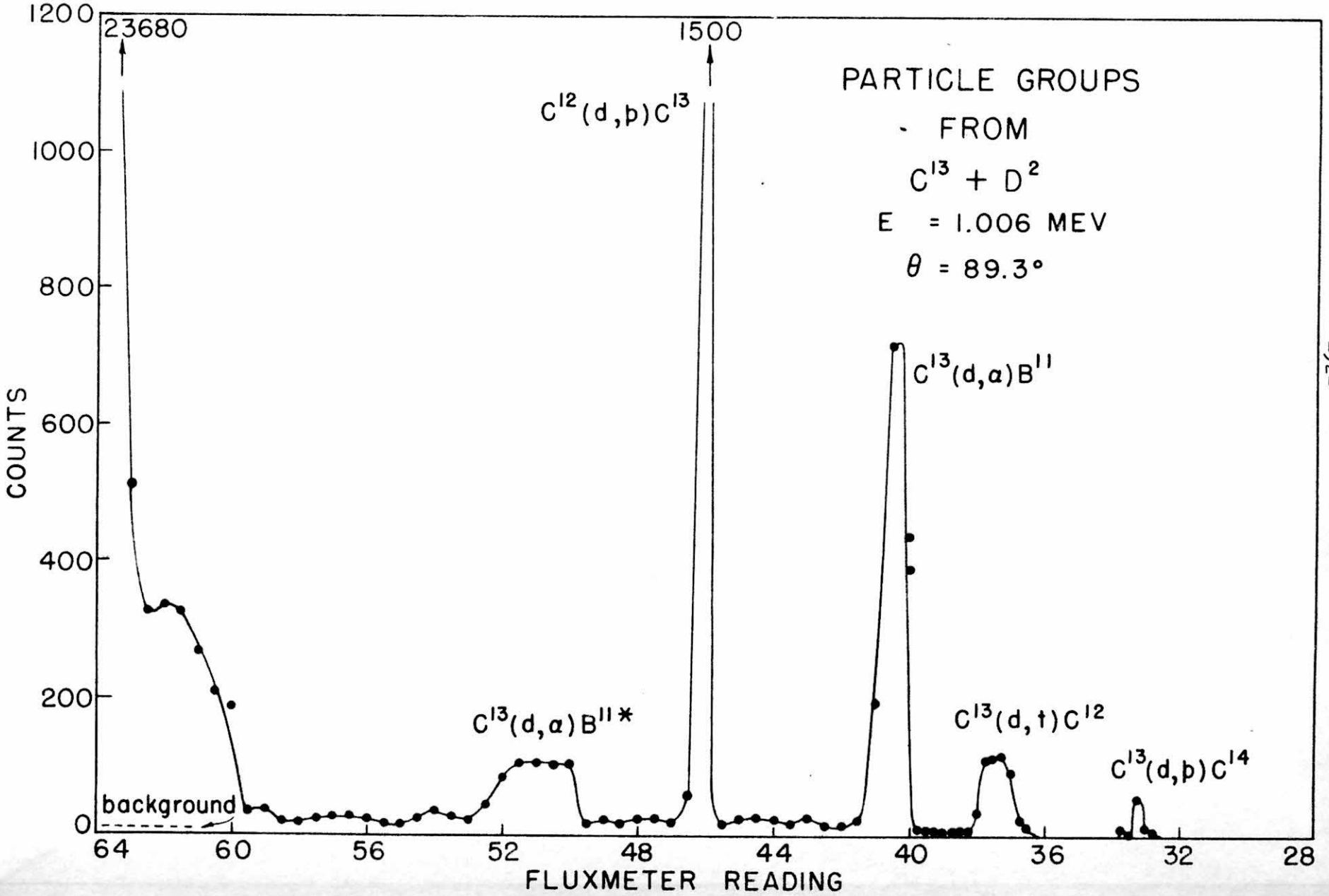
PARTICLE GROUPS
FROM
$C^{13} + D^2$
E = 1.006 MEV
θ = 89.3°
23680
1500
$C^{12}(d,p)C^{13}$
$C^{13}(d,\alpha)B^{11}$
$C^{13}(d,\alpha)B^{11}*$
$C^{13}(d,t)C^{12}$
$C^{13}(d,p)C^{14}$
background
COUNTS
FLUXMETER READING
0
200
400
600
800
1000
1200
64
60
56
52
48
44
40
36
32
28

Fig. 11.

Fig. 12.

REACTIONS WITH ACCURATELY KNOWN Q-VALUES

A = 1 to 20